Land Mobile Satellite Channel Measurements and Modeling

CHUN LOO, SENIOR MEMBER, IEEE, AND JOHN S. BUTTERWORTH

This paper, tutorial in nature, describes the effort of many investigators who have and still are conducting channel measurements and modeling for land mobile satellite communications. It is worth noting that at the time of this writing, land mobile satellite communications has come of age and is operational. Various channel measurement results, ranging from ultrahigh frequency to Ka-band, are given in this paper. Many statistical channel models and simplified models that have been developed are referred to. Some of the models are applicable to geostationary and nongeostationary communications satellites. A statistical model developed by Loo is described in detail, as well as its extension to modeling land mobile satellite communications at Ka-band. This was accomplished by including a Gaussian probability density function to account for weather conditions. Also, practical computer-generated statistical channel models are given. These computer models should facilitate the estimation of performance of satellite communications systems.

Keywords*—*Channel modeling, mobile communications and radio propagation, satellite communications.

I. INTRODUCTION

For the past 15 years, a great deal of work has been carried out on land mobile satellite (geosynchronous) channel measurements and modeling by researchers in various parts of the world. Land mobile satellite communications have come of age and are operational [1], [2], [4]–[6]. This paper provides a review of the effort on channel measurement and modeling over this period. Most of the material described here has been published in various scientific journals and/or conference proceedings.

We at the Communications Research Centre (CRC) began our propagation measurement program in the spring of 1981 during the Phase A (feasibility) and B (project definition) of the Canadian Mobile Satellite (MSAT) Program [9]. The objective of the measurement program was to provide engineering design data on excess path loss for a satellite communications system covering suburban and rural areas. Measurements were carried out at both the ultrahigh-frequency (UHF) band (800 MHz) and the L-band (1542 MHz) [10], [11]. Prior to our measurements, the only information published was on work by Hess, sponsored by the National Aeronautics and Space Administration (NASA), describing measurements made using the ATS-6 satellite [12].

From 1984 to 1987, the German Aerospace Research Center (DFVLR, now DLR) performed a series of propagation measurements at L-band (1.54 GHz) using Marecs [13]. Its measurements were conducted in several European cities with satellite elevation look angles ranging from 13° to 43°. Since about 1983, Goldhirsh and Vogel, supported by NASA, have carried out an extensive measurement program for land mobile satellite communications at UHF-, L-, S-, and Ka-bands [14]–[23]. Also, investigators from Europe [24]–[28], Japan [29]–[34], and Australia [35] have conducted propagation measurements for land mobile satellite communications in UHF-, L-, and S-bands. Recent interest in propagation measurements has been extended to Ka-band (20/30 GHz) for land mobile satellite communications for multimedia service. There have been a number of propagation measurements carried out using Olympus [37], [39], [43], Italsat [38], [42], [44], [45], and NASA's Advanced Communications Technology Satellite (ACTS) [40], [41].

In parallel with the propagation measurements, there was a great effort to develop statistical channel models based on measurements [13], [21], [43], [46]–[48], [62], [64], [50]–[60]. Some of the statistical models were extended to satellites with nongeosynchronous orbits [63], [65], [66]. In 1984, Loo developed a statistical model based on measurements for land mobile satellite communications. This model can represent a varying amount of shadowing and is mostly physically intuitive [46]. A little later, in 1986, Lutz *et al.* developed essentially a two-state model to represent shadowed and nonshadowed conditions for a given percentage of the time [13]. At about the same time, Stutzman *et al.* also did work on channel modeling and have developed a simplified log-normal shadowing model [48]–[50], [54]. In 1988, Goldhirsh and Vogel developed an empirical roadside shadowing model [21]. Also, Vogel and Hong have developed geometric analytic models [18]. Other investigators have extended these statistical models for applications to geosynchronous and nongeosynchronous

Manuscript received December 19, 1997.

The authors are with the Communications Research Centre, Ottawa, Ontario K2H 8S2 Canada.

Publisher Item Identifier S 0018-9219(98)04243-1.

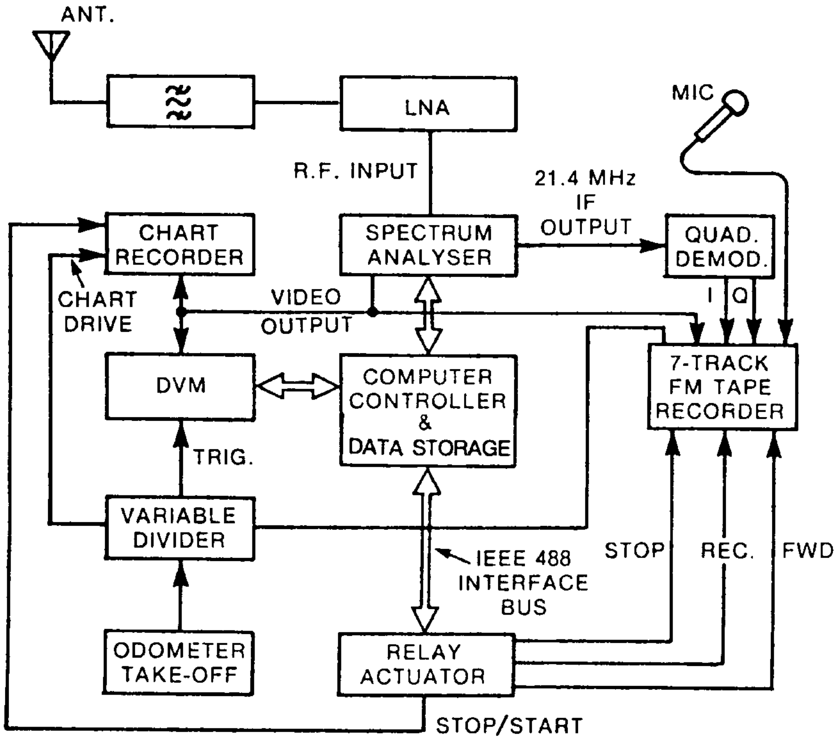

Fig. 1. Block diagram of the mobile laboratory equipment.

satellite communications [55]–[57], [61], [63]–[66]. More recently, Loo has extended his model for land mobile satellite communications at L-band to Ka-band [43].

This paper is organized in the following way. Section II describes propagation measurements at UHF- (800 MHz), L- (1542 MHz), and Ka-band (18.925 GHz). Statistical channel models and computer-generated models are given in Section III. Section IV summarizes the paper.

II. Propagation Measurement

There have been many investigators who conducted propagation measurements at UHF-, L-, S-, and Ka-band for land mobile satellite communications [13]–[42]. Some of their results will be highlighted in the following subsections. The emphasis, however, will be on results obtained at the CRC. For details on the results of many other investigators, the interested reader should refer to the references given.

A. Measurement Procedure

Fig. 1 shows the equipment used in the mobile laboratory for the UHF-band measurements [10]. The signal received by a conical log-spiral antenna was amplified and detected. Samples of the received signal strength were recorded in real time, and tape recordings were made of received signal amplitude and signal phase—"stored channel" recordings [67].

To simulate a satellite signal source, a helicopter was used to carry a transmitter package. An inverted conical log-spiral antenna housed the transmitter electronics and batteries. The effective isotropic radiated power (EIRP) was

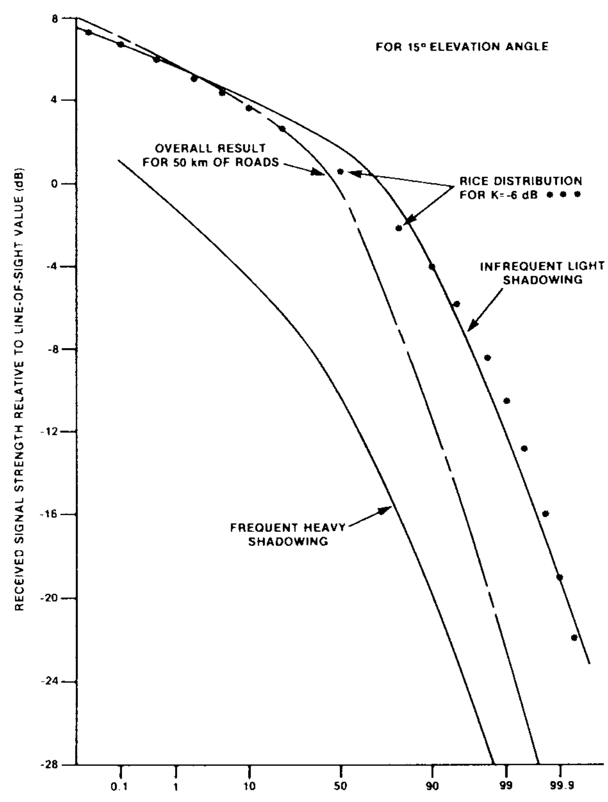

Fig. 2. Probability distribution functions of data measured at 870 MHz.

on the order of a few milliwatts. The total package weight of about 2 kg was carried by the helicopter, which kept pace with the mobile laboratory at a range of a few kilometers,

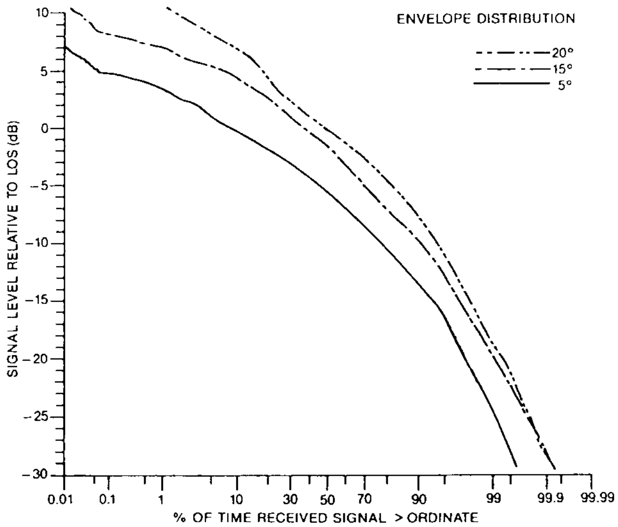

Fig. 3. Probability distribution of the signal envelope at several elevation angles; light shadowing; 870 MHz.

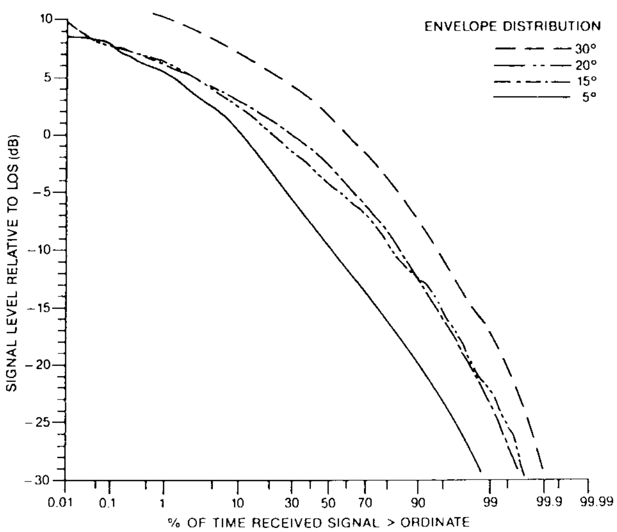

Fig. 4. Probability distribution of the signal envelope at several elevation angles; heavy shadowing; 870 MHz.

such that a constant relative bearing was maintained. This scheme allowed us to simulate various elevation angles with respect to the earth-to-satellite path.

For the L-band propagation measurement, the same mobile laboratory was used, except that the receive antenna was a drooping crossed dipole and the transmitter source was Inmarsat's Marecs A satellite [11]. Also, a fault detection scheme was incorporated in the measurement setup to avoid any accidental interference with operational traffic. The elevation angle from the ground terminal to the satellite was 19° for the L-band measurements.

For the Ka-band propagation measurements, different electronics were used compared to the L-band case [37]. An experimental 4.2-m Ka-band terminal was used to access the Olympus satellite [85]. The elevation angle to Olympus from Ottawa, Canada, was 14.2°. To measure the channel characteristics at Ka-band, a continuous-wave (CW) signal at a frequency of 28.0 GHz was transmitted from the

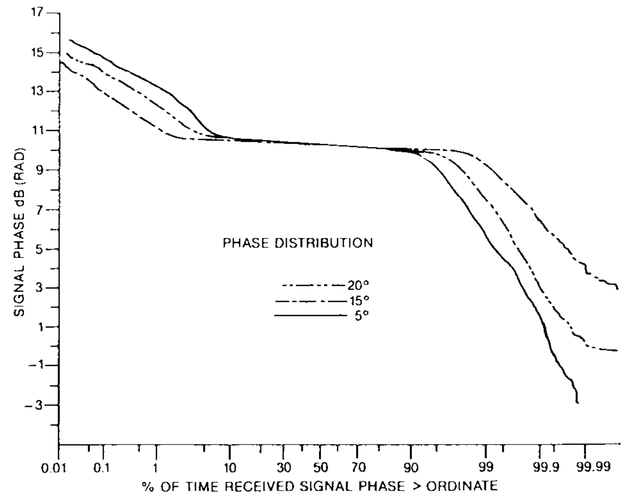

Fig. 5. Probability distribution of the signal phase at several elevation angles; light shadowing; 870 MHz.

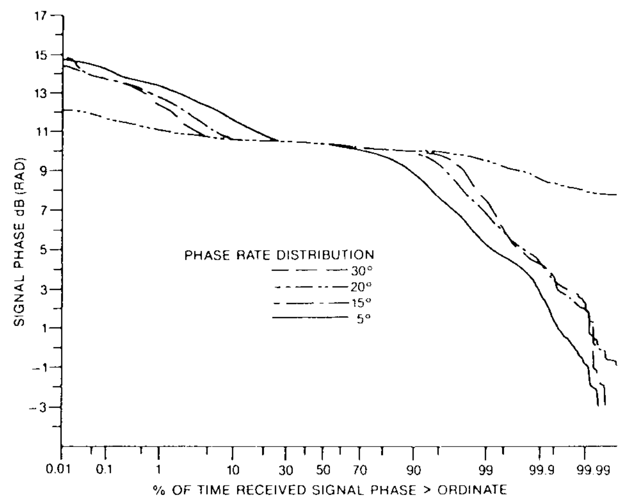

Fig. 6. Probability distribution of the signal phase at several elevation angles; heavy shadowing; 870 MHz.

4.2-m terminal and was received by the mobile terminal at a frequency of 18.925 000 GHz. Both the 4.2-m and the mobile terminals used double frequency conversion. A major part of the mobile terminal consisted of a recently developed suitcase terminal [86] and a standard gain horn antenna with a beamwidth of 10° at Ka-band. The suitcase terminal without the antenna was located inside the mobile laboratory, and the standard gain horn was mounted on its roof. The terminal interface of the CW signal was at an intermediate frequency (IF) of 70 MHz. The received CW signal at the mobile terminal was further down-converted to an IF of 4.8 kHz for storing on a digital audio tape recorder for subsequent analysis.

For the measured Ka-band data described in this paper, the mobile terminal was travelling at a speed of about 10 km/h in the direction of the satellite. At the beginning of the measurement, the mobile terminal was stationary, and the received CW data were recorded for the purpose of comparison to a moving terminal. One should note, however, that the effects of fading on the up- and downlink

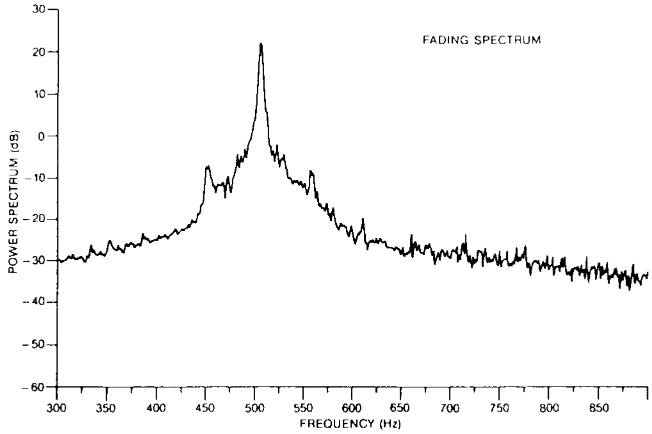

Fig. 7. Doppler spectrum; light shadowing at 5° elevation angle; 870 MHz.

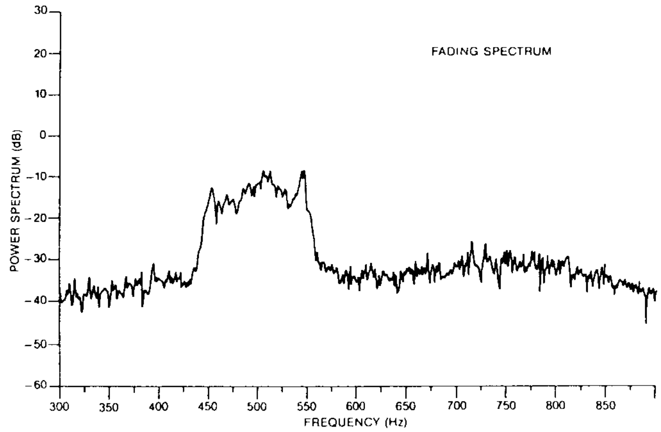

Fig. 9. Doppler spectrum; heavy shadowing at 5° elevation angle; 870 MHz.

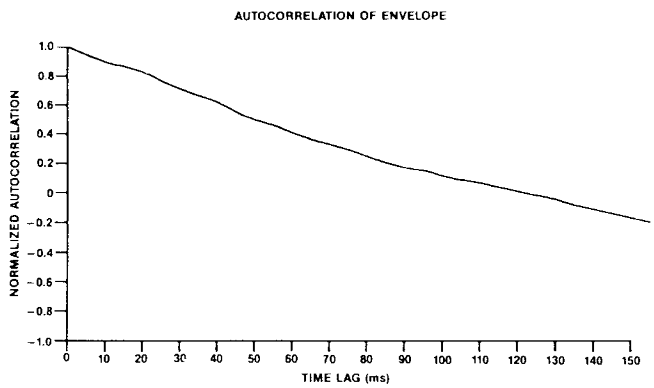

Fig. 8. Autocorrelation of signal envelope; light shadowing at 5° elevation angle; 870 MHz.

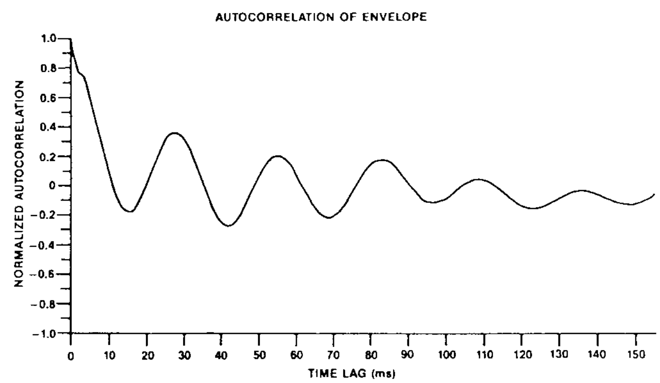

Fig. 10. Autocorrelation of signal envelope; heavy shadowing at 5° elevation angle; 870 MHz.

due to changing weather conditions were included in the data even though the mobile terminal was stationary.

B. Data Analysis Procedure

For the UHF-band (800 MHz) and L-band (1542 MHz) data analysis, the recordings of the in-phase and quadrature components of the received signal were sampled, digitized, and stored on diskettes for subsequent analysis by computer. The signal envelope and signal phase data were obtained by transforming the rectangular coordinates (in-phase, quadrature) to polar coordinates (envelope, phase). However, there was always a residual carrier frequency up to 1 kHz in the data stored on diskette. This carrier was due to the frequency difference between the transmitter carrier and the local oscillator. Before the data were analyzed, the residual carrier was frequency shifted down to dc. This was accomplished by means of the fast Fourier transform (FFT) algorithm [80] to determine the amount of frequency offset required prior to determining the probability density function of the signal envelope and phase. The transmitted carrier frequency and the local oscillator frequency differed because of drift and Doppler shift. Hence, it was not possible to analyze the signal phase due to fading and shadowing down to dc without analyzing the phase noise of the local oscillator.

For this reason, a 10-pole Butterworth bandpass attenuation characteristic with a passband between 30 and 320 Hz was used to filter the received signal phase spectrum prior to calculating its probability density function.

For the Ka-band data analysis [37], the received signal stored on digital audio tape at an IF of 4.8 kHz was quadrature demodulated to obtain its in-phase and quadrature components. From these components, one can readily obtain the signal envelope and signal phase components using a coordinate transformation as before.

C. UHF-Band Measurement

Several investigators have conducted propagation measurements in the UHF band, with the most extensive measurements having been carried out by Goldhirsh and Vogel [14]–[23]. Hess [12] conducted the UHF measurements using NASA's application technology satellite ATS 6. Measured results were obtained for elevation angles ranging from 19° to 43°. His results show that excess path loss, on the order of 25 dB, is typical in urban areas but decreases to under 10 dB in suburban/rural areas. Vogel and Goldhirsh have conducted measurements on shadowing from roadside trees using a remotely piloted aircraft. Their results show attenuation for a single tree, the average of the largest median of 16.1 dB, and the average of an

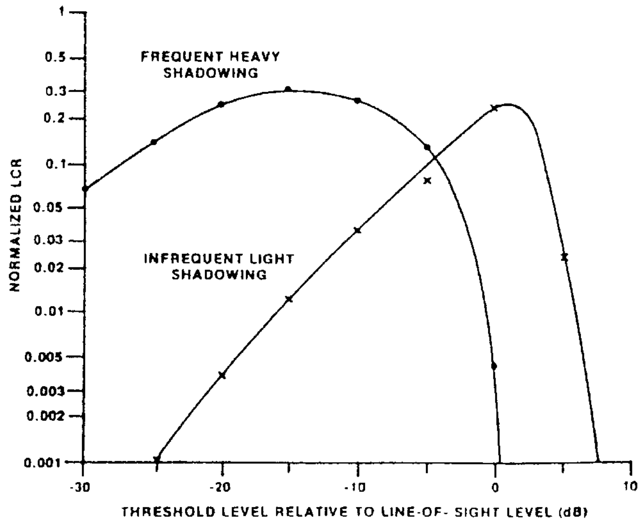

Fig. 11. Variation of normalized LCR; 870 MHz.

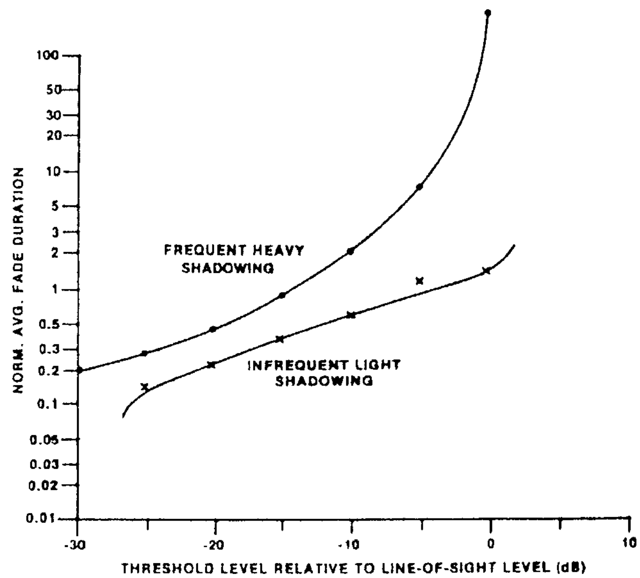

Fig. 12. Variation of normalized AFD; 870 MHz.

average median of 11.7 dB over a 10°–40° elevation angle [14], [15]. They have also conducted measurements over mountainous terrain (canyon), and their results show 1% and 5% levels of 4.8 and 2.4 dB on the average is exceeded, compared to 15 and 9 dB for roadside trees [16]. Percent level is defined as the percentage of time that a faded signal is exceeded. More results by Goldhirsh and Vogel on the effect of trees in full bloom and the dependence of fade distribution as a function of elevation angles are given in [17].

Bundrock and Harvey conducted measurements for an Australian land mobile satellite system. They also used a helicopter as a platform for their transmitter. Their results show for an elevation angle of 45° and for a 10% level a value of 4.2 and 6.6 dB for a 35% and 85% tree density areas, respectively [35].

Next, we describe the CRC measured results [10], [68]. The measurements were obtained along several roads in West Carleton Township, just west of Ottawa, Canada, in September 1982, while the deciduous trees were still in leaf. In area, West Carleton is 35% wooded, the rest being clear land (40% is farmland). Fig. 2 shows the signal envelope probability distribution function for an elevation angle of 15°. The upper curve corresponds to infrequent light shadowing when traversing cleared land. The only shadowing objects are roadside power poles and occasional trees, etc. For this case, the distribution is close to Rician. However, the value of the parameter K, a ratio of multipath power to line-of-sight (LOS) power, for best fit has risen from -12 dB , typical under clear conditions, to about -6 dB. The lower curve indicates the results obtained when traversing a densely wooded area, with trees extending close to the roadside. With a median value of 10.5 dB, this would represent an outage for a satellite system. The overall result is shown by the middle curve. If 90% area coverage were required in West Carleton, at a service elevation angle of 15°, an excess loss margin of 11.5 dB would be required. Fig. 3 shows the probability distribution of the received signal envelope for the case of light shadowing at elevation angles of 5°, 15°, and 20° [47]. The results show that signal level decreases with reduced elevation angle. Similar results were obtained for the case of heavy shadowing, as shown in Fig. 4. Several observations can be made on the results of Figs. 3 and 4. The difference in the probability distributions of the signal envelope for 15° and 20° elevation is relatively small. Signal-level spread for various elevation angles is much larger for heavy shadowing than it is for light shadowing. For example, for 95% of the time, the signal level lies between -17 and -11 dB for light shadowing and between -23 and -11 dB for heavy shadowing, giving a spread of 6 and 12 dB for light and heavy shadowing, respectively. Also, for the case of heavy shadowing at an elevation angle of 30°, the results as shown in Fig. 4 are consistent, since there is less shadowing (blockage) by trees for higher elevation angles than there is for lower elevation angles. Fig. 5 shows the signal phase distribution at 870 MHz for the case of light shadowing at several elevation angles. The results show that, for 5–95% of the time, the signal phase distribution is approximately independent of elevation angle. On the other hand, the tails of the distribution increase with decreasing elevation. For the case of heavy shadowing shown in Fig. 6, the phase variations are much larger with decreasing elevation angle. Also, the percentage of time where the signal phase distribution is approximately independent of the elevation angle is reduced, being 20–80%.

Fig. 7 shows a signal envelope spectrum for the case of light shadowing at an elevation of 5° [87]. Light shadowing is generally experienced when travelling through sparsely wooded areas. The spectrum shows that there was clearly an LOS component at a frequency of about 500 Hz. The peak-to-peak Doppler shift was about 114 Hz. At a nominal carrier frequency of 870 MHz and a peak Doppler shift of 57 Hz, the mobile laboratory was travelling at about 70 km/h when the data were taken. Fig. 8 shows the autocorrelation function of the same signal. This was obtained by

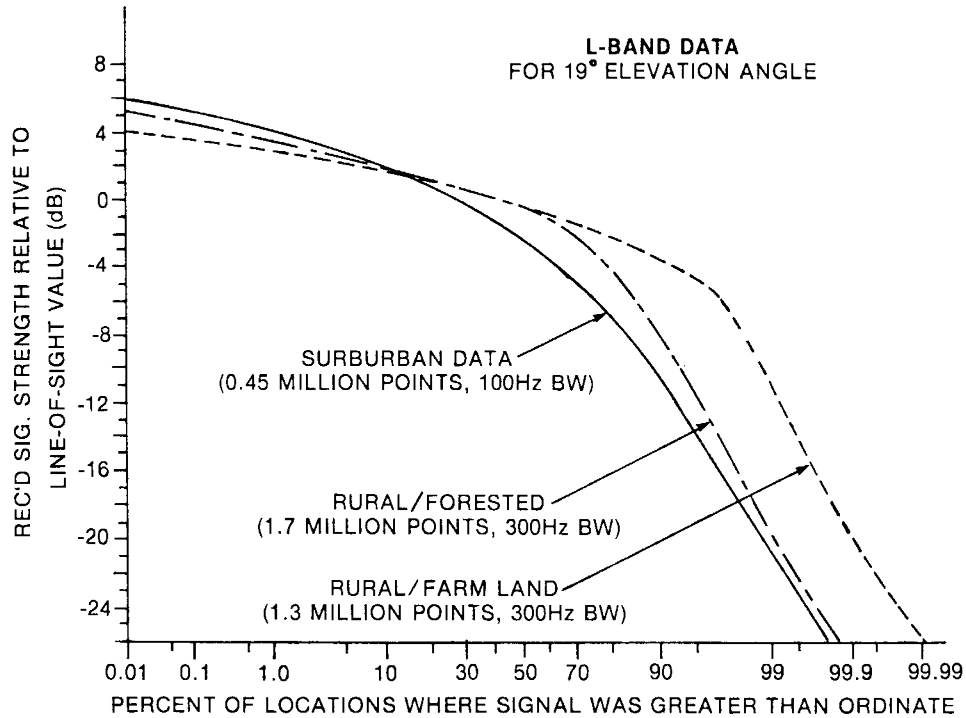

Fig. 13. Probability distribution of signal envelope; 1542 MHz.

first frequency shifting the residual carrier down to dc and then performing an inverse Fourier transform on the data. The results show that the autocorrelation function decreases almost linearly with time lag. This is due mainly to the presence of a strong LOS component. For the case of heavy shadowing at an elevation of 5°, a signal envelope spectrum is shown in Fig. 9. Heavy shadowing is experienced when travelling through densely wooded areas. The spectrum shows that the LOS component, which has a frequency of about 510 Hz, has almost disappeared. Also, the peak-to-peak Doppler frequency was 107 Hz, indicating that the vehicle was travelling at about 66 km/h when this measurement was made. Fig. 10 shows the autocorrelation function for this case. It consists of a main lobe, decreasing in an oscillatory manner with time lag, indicating a lack of the LOS component.

Figs. 11 and 12 show second-order statistics of the channel in terms of level crossing rate (LCR) and average fade duration (AFD) for infrequent light shadowing and frequent heavy shadowing [68]. These statistics are of importance in the selection of voice-processing and modulation methods.

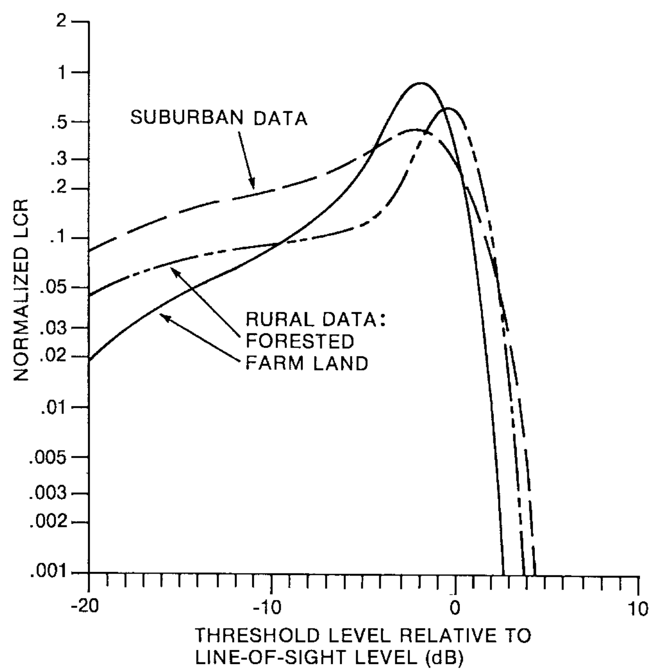

Fig. 14. Variation of normalized LCR; 1542 MHz.

D. L-Band Measurement

There were many more investigators who conducted measurements at L-band than at UHF-band. The reason for this was simple; L-band was the allocated frequency band for land mobile satellite communications systems. Hess had shown in his results that the excess path-loss difference between UHF- and L-band is generally negligible [12]. This was confirmed by Vogel and Goldhirsh's results, which showed the difference to be 1–1.3 dB [18]. Matsumoto *et al.* [30] conducted L-band propagation measurement in Kyoto, Japan, using ETS-V. Their results show that for a 10% level, which represents that the faded signal is exceeded, the fade is 27.5 dB at an elevation angle of 46°. Using a light aircraft as the transmitter platform, Renduchintalia *et al.* [24] have also conducted measurements at several elevation angles and under different terrain conditions. For a 10% level and at an elevation of 40°, the fades are 5.6, 6.0, and 16.4 dB for tree shadowed, suburban, and dense urban areas, respectively. However, at an elevation of 60°

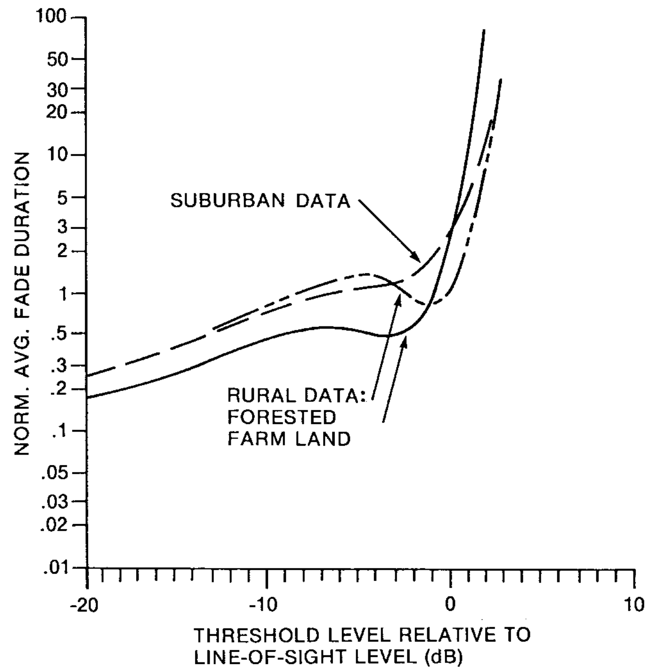

Fig. 15. Variation of normalized AFD; 1542 MHz.

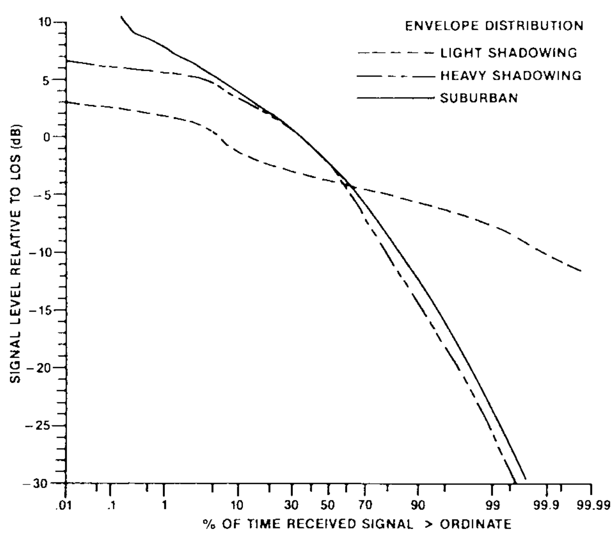

Fig. 16. Probability distribution of the signal envelope at 20° elevation angle; light and heavy shadowing and suburban area; 1542 MHz.

and for a 10% level, the fades are 4, 1, and 14.2 dB for tree shadowed, suburban, and dense urban areas, respectively. Lutz *et al.*'s [13] results show, for an elevation of 24° and at a 9% level, that the faded signal is more than 10 dB below an unfaded level for a highway environment. For urban areas (Munich, Germany) and for the amount of a 10-dB fade as before, the probability level is at 60%, that is, at a 40% level.

Using ETS-V, at an elevation of 47° and on main roads of relatively smaller cities (pop. 50 000–400 000), Yoshikawa and Kagohara's [34] results show that at a 10% level, the received signal level is 3 dB lower than the unfaded signal. Using Marecs-B2 and at an elevation of 21.2°, Vogel and

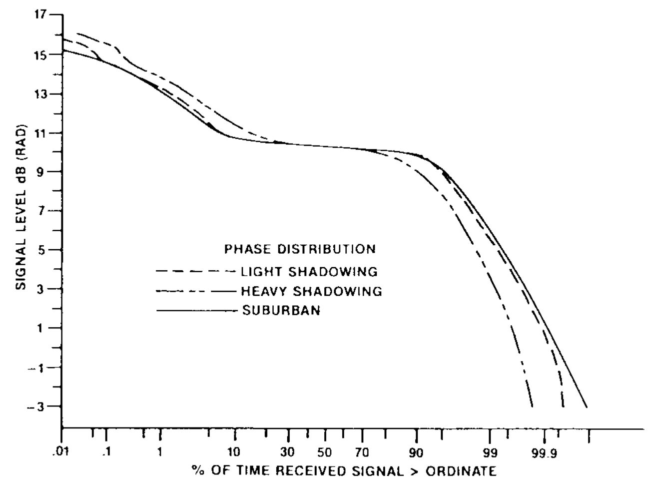

Fig. 17. Probability distribution of the signal phase at 20° elevation angle; light and heavy shadowing and suburban area; 1542 MHz.

Goldhirsh's [19], [22] results show that for a 20% level, the observed fades are 15, 11.5, and 9 dB for a four-lane highway 75% lined with trees and 35% along the center median, a suburban two-lane road, and a rural two-lane highway respectively. For a range of elevation angles from 7° to 14°, their results show that for a 1% level, fading can exceed 7 dB for rolling, hilly terrain and 25 dB for tree shadowing.

During the summer and using a helicopter to mount a transmitter to simulate an elevation of 60°, Butt *et al.*'s [25] results show that for a 10% level, the observed fades are 5.0 and 7.5 dB for suburban and wooded areas, respectively. Obara and Tanaka [31] conducted measurement with ETS-V at a range of elevations, between 40° to 50°, and on an expressway. Their results show a fade of 5 dB for a 10% level. Using a light aircraft to mount a transmitter and at an elevation of 40°, Smith *et al.* [26] obtained results that show, for a 10% level, that the fades are 3.5, 5.5, and 5.9 dB for suburban, urban, and tree shadowed areas, respectively.

Using Marecs-B2 and at an elevation of 39°, Benarroch and Mercader [27] obtained results for a 10% level as 10.6, 2.0, and 2.0 dB for urban, suburban, and rural areas, respectively. Also, for a 10% level, but at an elevation of 13°, the fades are 13, 11, and 9 dB for urban, suburban, and rural areas, respectively. Kanatas *et al.* [28] have also conducted measurements using a helicopter to mount a transmitter and to simulate an elevation of 60°. Their results show, for a 10% level, that fades range from 21.8 to 25.8 dB for an urban environment with narrow streets and high buildings.

The CRC measured results are described next [11], [47], [69]. Fig. 13 shows the cumulative distribution of the received signal envelope for three different environmental conditions. These distributions were obtained from measurements taken at 2.5-cm intervals along the route. The rural data shown were gathered near Eganville (45° 32′N, 77° 0′W), approximately 115 km northwest of Ottawa, on roads passing through predominantly forested, hilly terrain. The elevation angle to the satellite was approximately 18°.

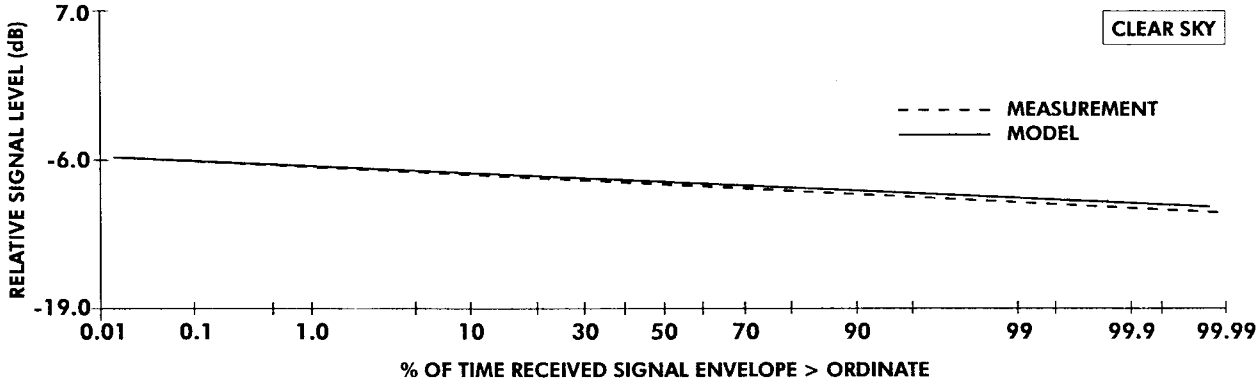

Fig. 18. Signal envelope model and measurement; clear sky conditions; 18.925 GHz.

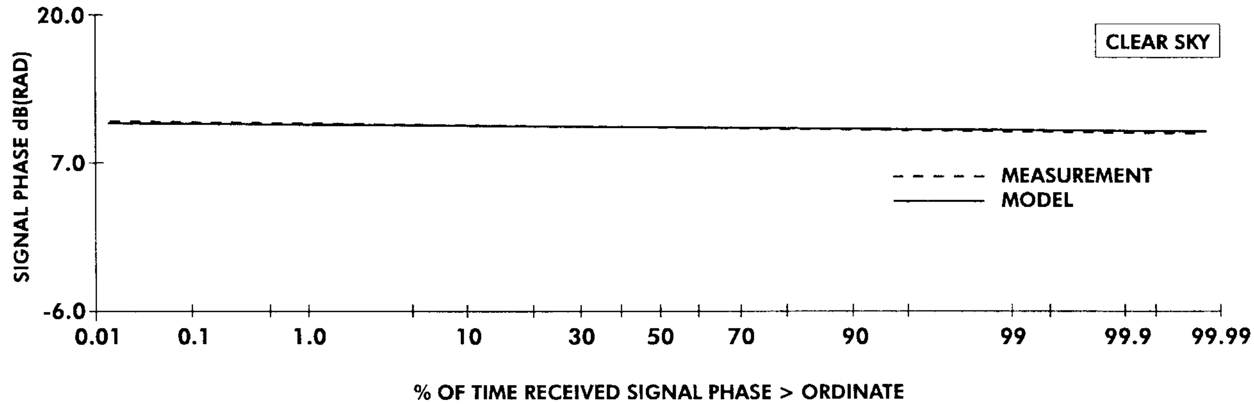

Fig. 19. Signal phase model and measurement; clear sky conditions; 18.925 GHz.

The forest was a mixture of deciduous and coniferous trees. The suburban data were gathered within a residential area of Ottawa, on streets bordered by one- and two-story homes, typical of North American city suburbs. The elevation angle to the satellite was 19°. The third curve shown was obtained over a route just south of Ottawa where an LOS component was mostly available, with the only obstructions being telephone or power line poles and very infrequent roadside trees. For example, for a 10% level, the results show that the fades are 3.0, 7.2, and 10.0 dB for rural, tree shadowed, and suburban areas, respectively. Other values can be obtained from Fig. 13.

Figs. 14 and 15 show the variation of normalized LCR and normalized AFD [70] for the three categories of data. The previous results on signal envelope fading as shown in Fig. 13 were derived from the video output of the mobile laboratory where no signal phase information was available. To obtain signal phase information, one needs to analyze the "stored channel" data. A portion of this data was selected, and the signal envelope fading is shown in Fig. 16 for light and heavy shadowing of a rural as well as a suburban area. The results show that the difference in signal strength between light and heavy shadowing is relatively large. For example, for a 10% level, the fades are 5.2, 11.8, and 13.9 dB for light shadowing, suburban, and heavy shadowing, respectively. These results are a couple of decibels worse than the video output. Fig. 17 shows the signal phase data. The results shown are similar to the UHF-band case.

E. Ka-Band Measurement

Some propagation measurements at Ka-band (20/30 GHz) have been carried out by several investigators [36]–[38], [40]–[43], [45], and their results are highlighted in this subsection. Vogel and Goldhirsh have conducted static tree attenuation measurements at 20 GHz and at an elevation of 30° through a mature pecan tree with and without leaves. Their results show median fades exceeding 23 and 7 dB for conditions with and without leaves, respectively, and the corresponding 1% probability fades were 43 and 25 dB. Pinck and Rice have conducted measurements using ACTS at an elevation of 46°. Their results show that for a 10% level, the fades are 0.8, 3.5, and 29.5 dB for lightly, moderately, and heavily shadowed suburban areas, respectively. Additional results are given in their paper [41].

Damosso *et al.* have used Italsat to conduct their measurements. Their results on attenuation due to vegetation and on frequency of occurrence between urban and suburban areas are described in their paper [38]. Borghino *et al.* [42] have also used Italsat to conduct their measurements at an elevation of 37.8°. Their results show attenuation of 15–20 and 5–9 dB for trees with and without leaves, respectively. Similar results were obtained by D'Amato *et al.* [44]. Using Italsat, Buonomo *et al.* [45] have conducted measurements over a range of elevation angles, 30–35°. Their results show that for a 10% level, the fades are 0.9, 7.2, 9.8, 10.1, and

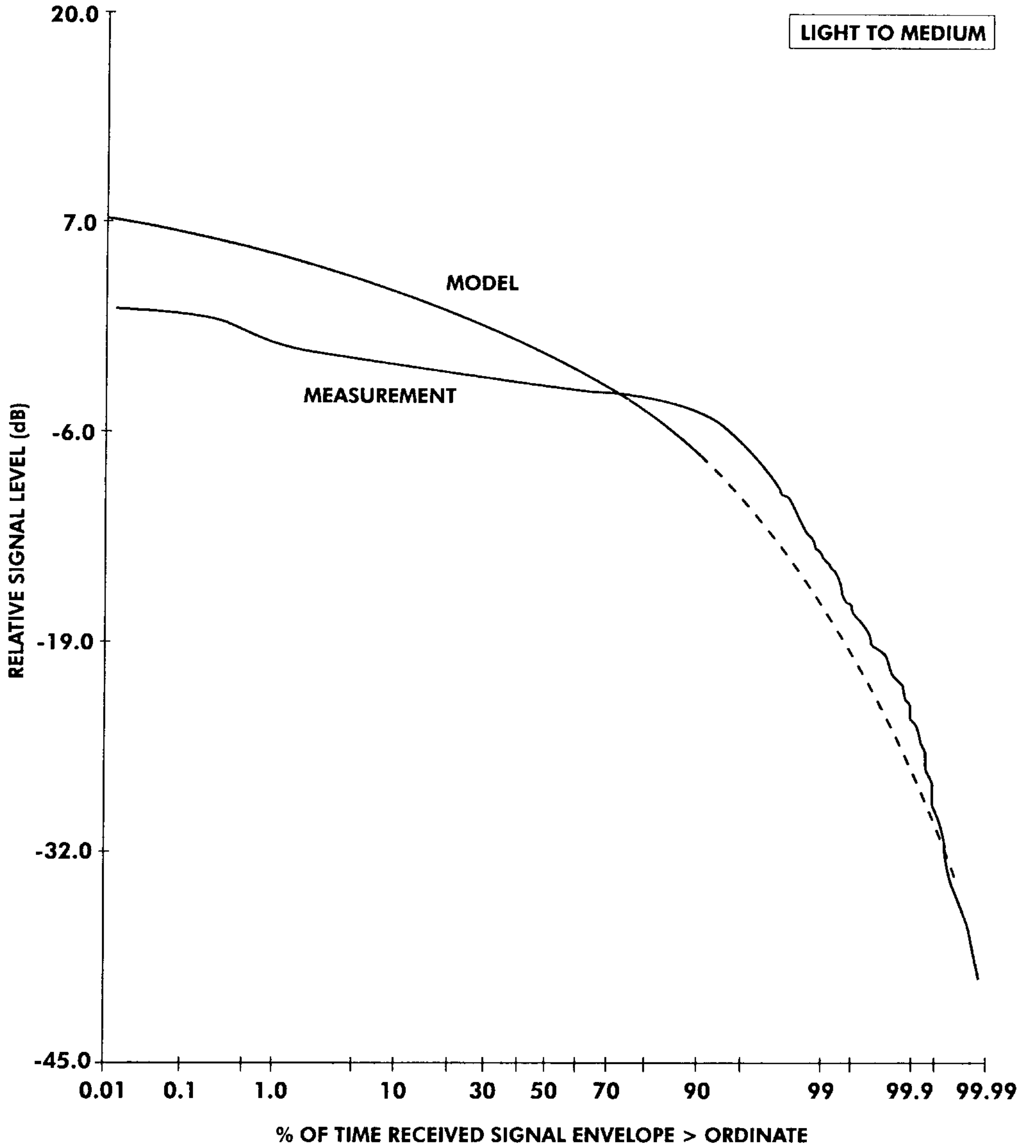

Fig. 20. Signal envelope model and measurement; light to medium shadowing; 18.925 GHz.

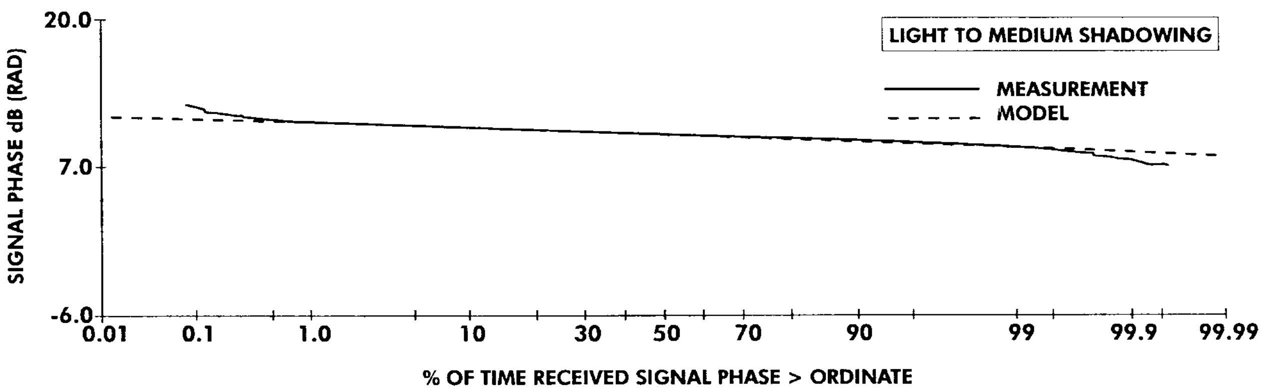

Fig. 21. Signal phase model and measurement; light to medium shadowing; 18.925 GHz.

21.8 dB for open, suburban, mixed, tree shadowed, and urban areas, respectively, and for a 1% level, the fades are 9.1, 16.3, 15.6, 17, and 26.6 dB, respectively.

Propagation measurements conducted at CRC using Olympus are described next [37], [43]. The elevation angle to Olympus from Ottawa, Canada, was 14.2°. The Ka-band frequency used was 18.925 GHz. Vehicular speeds were about 10–20 km/h and travelling in the direction of the satellite. Before describing the Ka-band measurements under mobile conditions, one should note that the effect

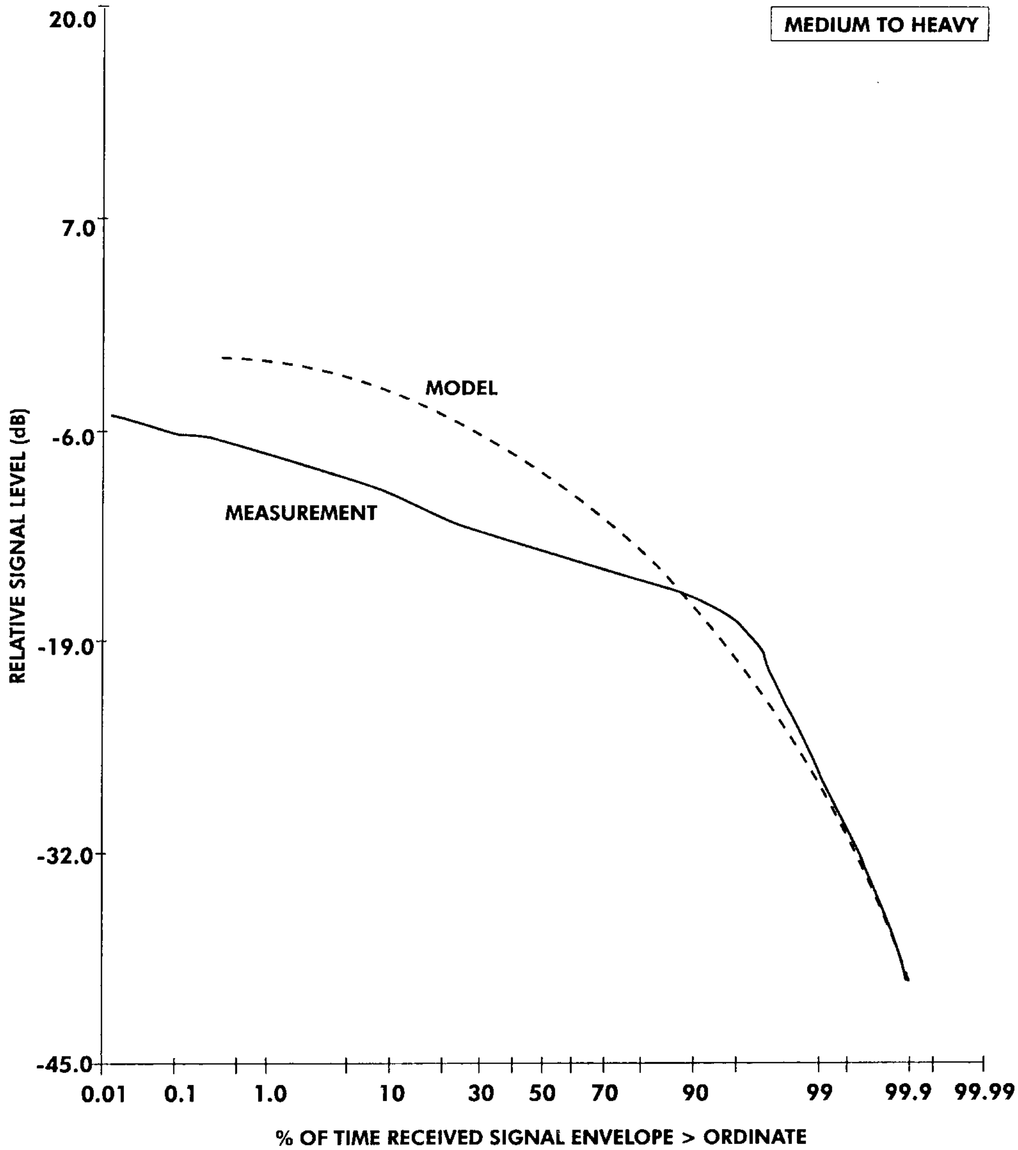

Fig. 22. Signal envelope model and measurement; medium to heavy shadowing; 18.925 GHz.

of fading on the up- and downlink due to changing weather conditions were included in the data. Results to be described in a mobile environment were recorded under cloudy with sunny break conditions, which represented almost clear sky conditions. The temperature was 23°C with 66% humidity. Figs. 18 and 19 show the received signal envelope and signal phase probability distribution under clear sky conditions. Figs. 20 and 21 show the probability distribution of signal envelope and signal phase for light to medium shadowing conditions. Also, Figs. 22 and 23 show results of medium to heavy shadowing for the signal envelope and signal phase probability distributions. Figs. 24 and 25 show results of heavy shadowing for the signal envelope and signal phase probability distributions. One should note that the dashed (– – –) curves represent statistical models that will be described in the next section. To illustrate extreme shadowing conditions, Fig. 26 shows a photograph of a roadside tree that can cause it. There is nearly no fading when the received antenna was not blocked by the tree. However, there is heavy shadowing when the antenna was blocked. For this case, the signal envelope and signal phase versus time are shown in Figs. 27 and 28, respectively. Referring to Figs. 20, 22, and 24, for a 10% level, the fades are 4.3, 16.4, and 17.3 dB for light to medium, medium to heavy, and heavy shadowing, respectively; and for a 1% level, the fades are 13.8, 28.1, and 31.1 dB, respectively.

F. Signal Phase Jitter

Results of signal phase jitter and random frequency modulation (FM) can be obtained from the signal phase probability density functions [47]. Tables 1 and 2 show results for an 870-MHz signal at several elevation angles for the cases of light and heavy shadowing, respectively. The results show that phase jitter variation and random FM tend to increase with decreasing elevation angles for both light and heavy shadowing. Phase jitter and random FM for

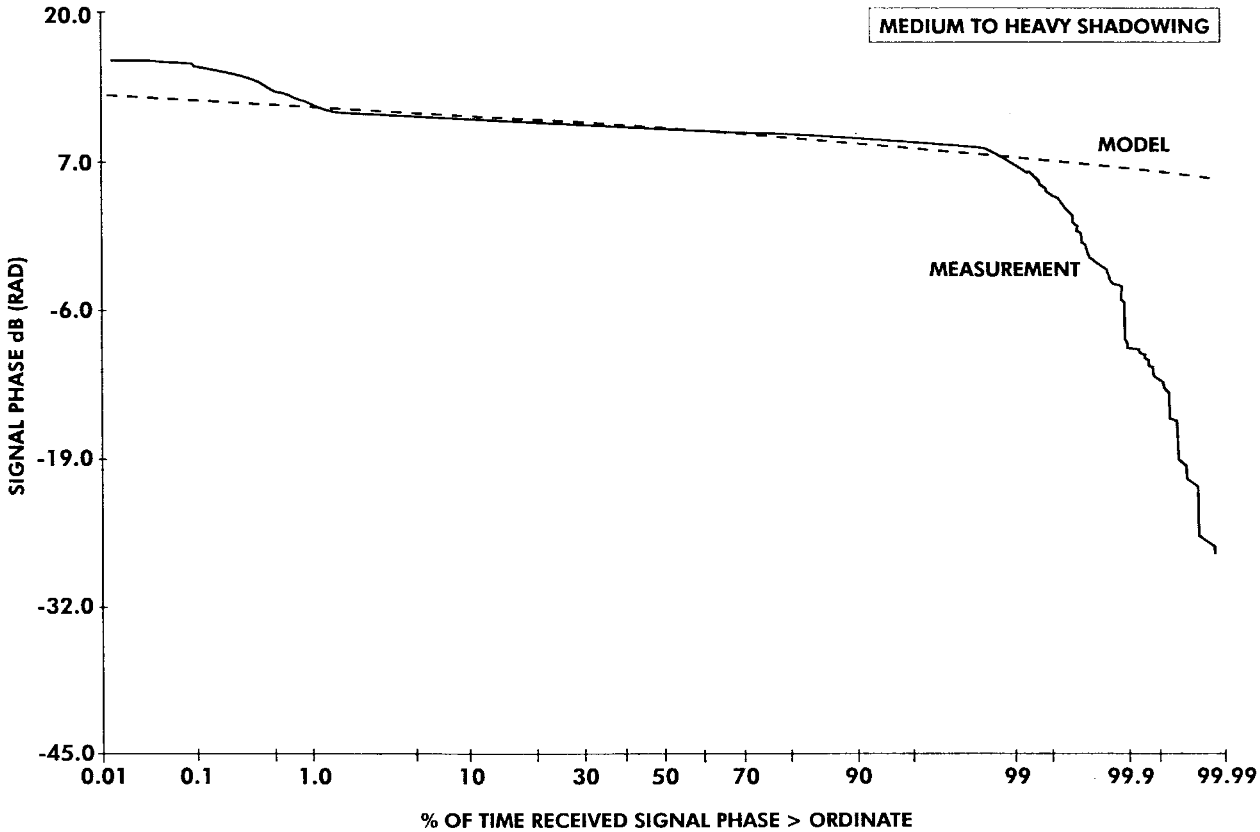

Fig. 23. Signal phase model and measurement; medium to heavy shadowing; 18.925 GHz.

a signal at 1542 MHz are shown in Table 3. These values are larger than those for 870 MHz. Phase jitter in terms of signal phase variance caused by weather conditions at Ka-band (18.925 GHz) is shown in Table 4. These results show that phase jitters are largest in rain. One can also use the values given in Table 4 to model the signal phase variation due to various weather conditions.

III. Statistical Models for the Land Mobile Satellite Channel

This section describes the essential results of statistical models for a land mobile satellite channel. More details are given in [43], [46], and [47]. For other models, the interested reader should refer to the references given.

A. Statistical Model for the L-Band Channel

The model assumes that the LOS component under foliage attenuation (shadowing) is log-normally distributed and that the multipath effect is Rayleigh distributed. Consider the sum of a log-normally distributed random phasor and a Rayleigh phasor [71]

$$r\exp(j\theta) = z\exp(j\phi_o) + w\exp(j\phi) \tag{1}$$

where the phase ϕ_o and ϕ are uniformly distributed between 0 and 2π, z is log-normally distributed, and w has a Rayleigh distribution. The signal envelope probability density function for the mobile satellite channel is

$$p(r) = r\Big/\left(b_0\sqrt{2\pi d_0}\right)\int_0^\infty 1/z\exp\left[-(\ln z-\mu)^2/2d_0 - \left(r^2+z^2\right)/2b_0\right] \cdot I_0(rz/b_0)\,dz \tag{2}$$

where $\sqrt{d_0}$ and μ are the standard deviation and mean of the log-normal probability density function, respectively. b_0 represents the average scattered power due to multipath and $I_0(\cdot)$ is the modified Bessel function of zeroth order. The following description refers to (1).

When z is constant and $z = A$, that is, a clear LOS component with no shadowing but with multipath fading, the signal envelope probability density function is Rician and is given by

$$p(r) = r/b_0\exp\left[-(r^2+A^2)/2b_0\right]I_0(rA/b_0). \tag{3}$$

When there is shadowing (z) but no multipath fading ($w = 0$), the signal probability density function is log-normal (Gaussian distribution in $\ln$ scale) and is given by

$$p(r) = 1/\left(r\sqrt{2\pi d_0}\right)\exp\left[-(\ln r-\mu)^2/2d_0\right]. \tag{4}$$

When there is no shadowing and no LOS component ($z = 0$) the signal envelope probability density function is Rayleigh distributed and is given by

$$p(r) = r/b_0\exp\left(-r^2/2b_0\right). \tag{5}$$

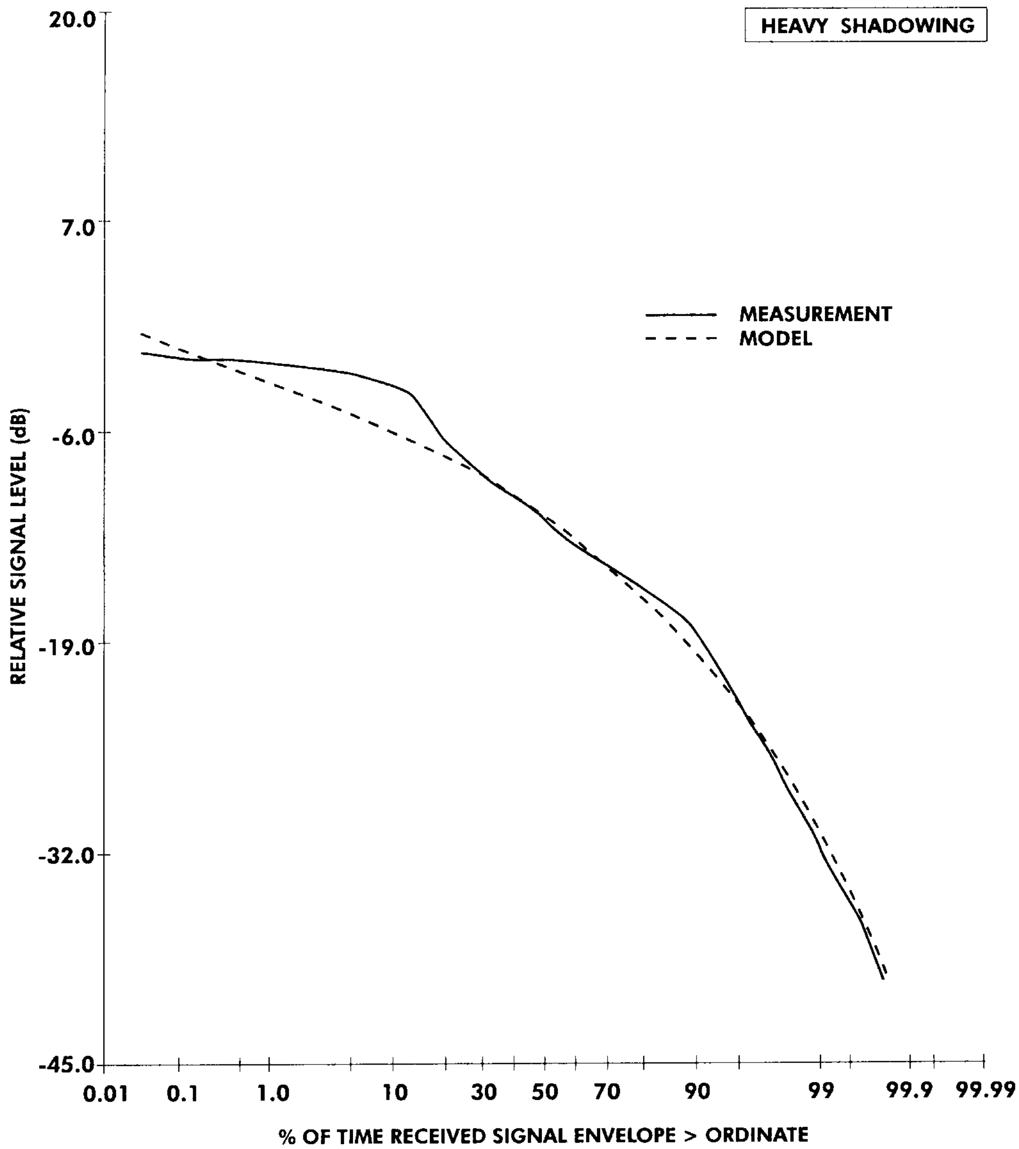

Fig. 24. Signal envelope model and measurement; heavy shadowing; 18.925 GHz.

The above description illustrated that (1) can represent various fading channel scenarios.

It is well known that the signal envelope probability density function of the model facilitates the calculation of fade margins in the designs of communications systems. Results of LCR and AFD, which are second-order statistics, provide information relevant to modem designs and error-correction techniques. Expressions of LCR (N_R) and AFD (T_N) have been obtained for the land mobile satellite channel, and these are given below [46]

$$N_R = \sqrt{2\pi}\sqrt{1-\rho^2}b_0\frac{\left(b_0+2\rho\sqrt{b_0d_0}+d_0\right)^{1/2}}{b_0(1-\rho^2)+4\rho\sqrt{b_0d_0}}p(r) \quad (6)$$

where ρ is the correlation coefficient

$$T_N = \frac{1}{N_R}\int_0^R p(r)\,dr. \quad (7)$$

Equations (6) and (7) represent normalized LCR and AFD, and the normalizing factor is maximum Doppler-shift frequency.

For the received signal phase model, ϕ is found to be approximately Gaussian when compared with results derived from experimental data [47]

$$p(\phi) = 1/\left(\sqrt{2\pi}\sigma\right)\exp\left[-(\phi-m)^2/2\sigma^2\right] \quad (8)$$

where m and σ are the mean and standard deviation of the Gaussian random process and a typical range of σ is 0.36–0.52 [88].

For the signal envelope statistical model, Fig. 29 shows a comparison of the cumulative distribution function for the received signal envelope calculated using the following equation:

$$p(r > R) = 1 - \int_0^R p(r)\,dr \quad (9)$$

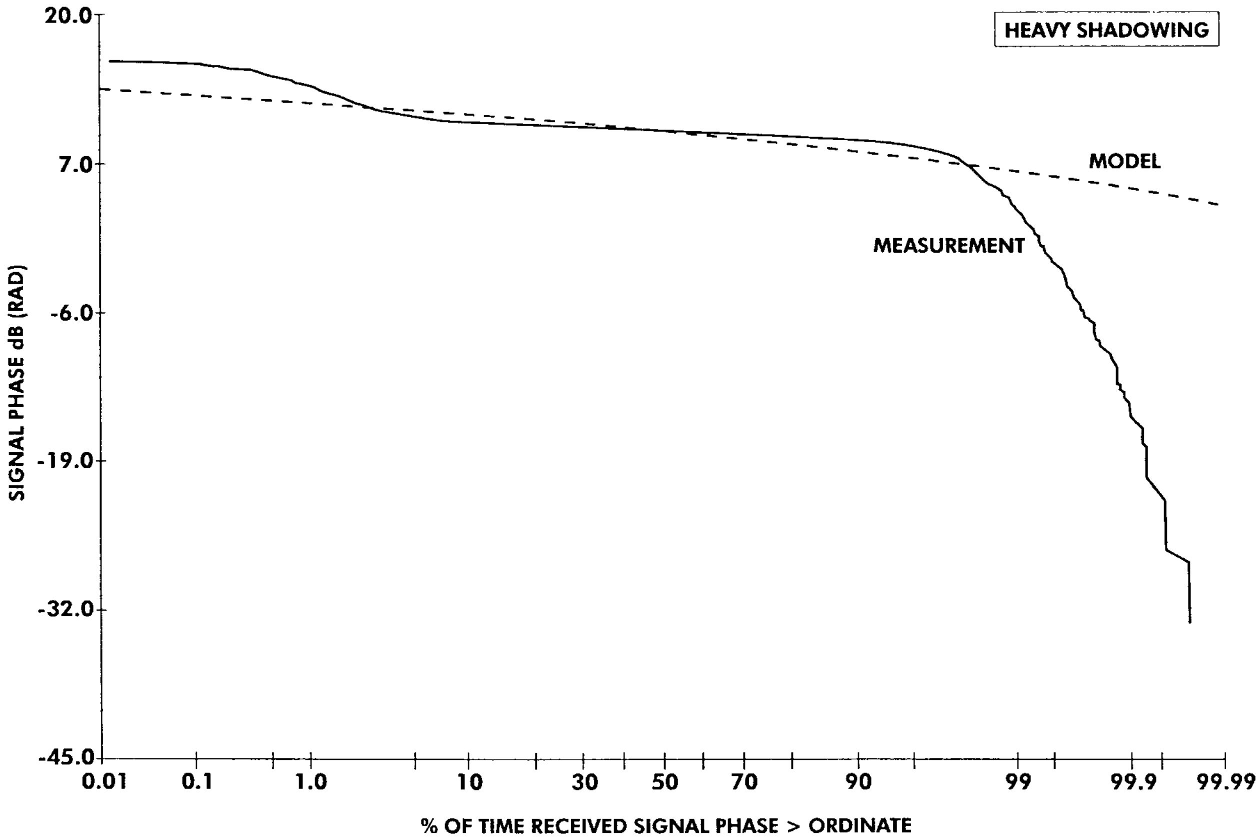

Fig. 25. Signal phase model and measurement; heavy shadowing; 18.925 GHz.

Fig. 26. A typical roadside tree that can cause heavy shadowing.

and the values derived from measurements for infrequent light shadowing (sparse tree cover), frequent heavy shadowing (dense tree cover), and overall results (the combined results of light and heavy shadowing). For the case of infrequent light shadowing, the model shows the best fit around the median region and some deviation near the tails of the distribution. Generally, the results of the model showed a slightly higher shadowing effect than those from measured data. For the case of frequent heavy shadowing, the results of the model show reasonably good agreement with measured values throughout the fading range. For the combined results, the fit was poor about the median but reasonably good in the weak signal range, which is most important for fade margin calculations. The model parameters were obtained by trial and error to fit the measured values. These parameters are given in Table 5.

Fig. 30 shows values for the LCR calculated using (6) for the case of infrequent light shadowing. The results show that the maximum LCR occurs when there is no correlation between the rate of change of the envelope due to multipath and that due to shadowing. Measured values [11] for this case are also shown. These results indicate that the model gives a good indication of the LCR when high correlation, $\rho = 0.5$–0.9, between multipath and shadowing is assumed. The figure also indicates that there is a bound on the LCR when the signal is large. Fig. 31 shows a plot of the AFD calculated from the model and from measurements. Application of the model results in a good approximation to the AFD anticipated on a mobile satellite link. For low signal levels, the two curves compare reasonably well. These results also show that the best fit is obtained when ρ is large.

B. Statistical Model for Ka-Band (20/30 GHz) Channel

From the results described in [37] and [43], it is shown that the general statistical model (2) for L-band can be applied to a land mobile satellite channel at Ka-band with different parameters. For fixed or mobile satellite

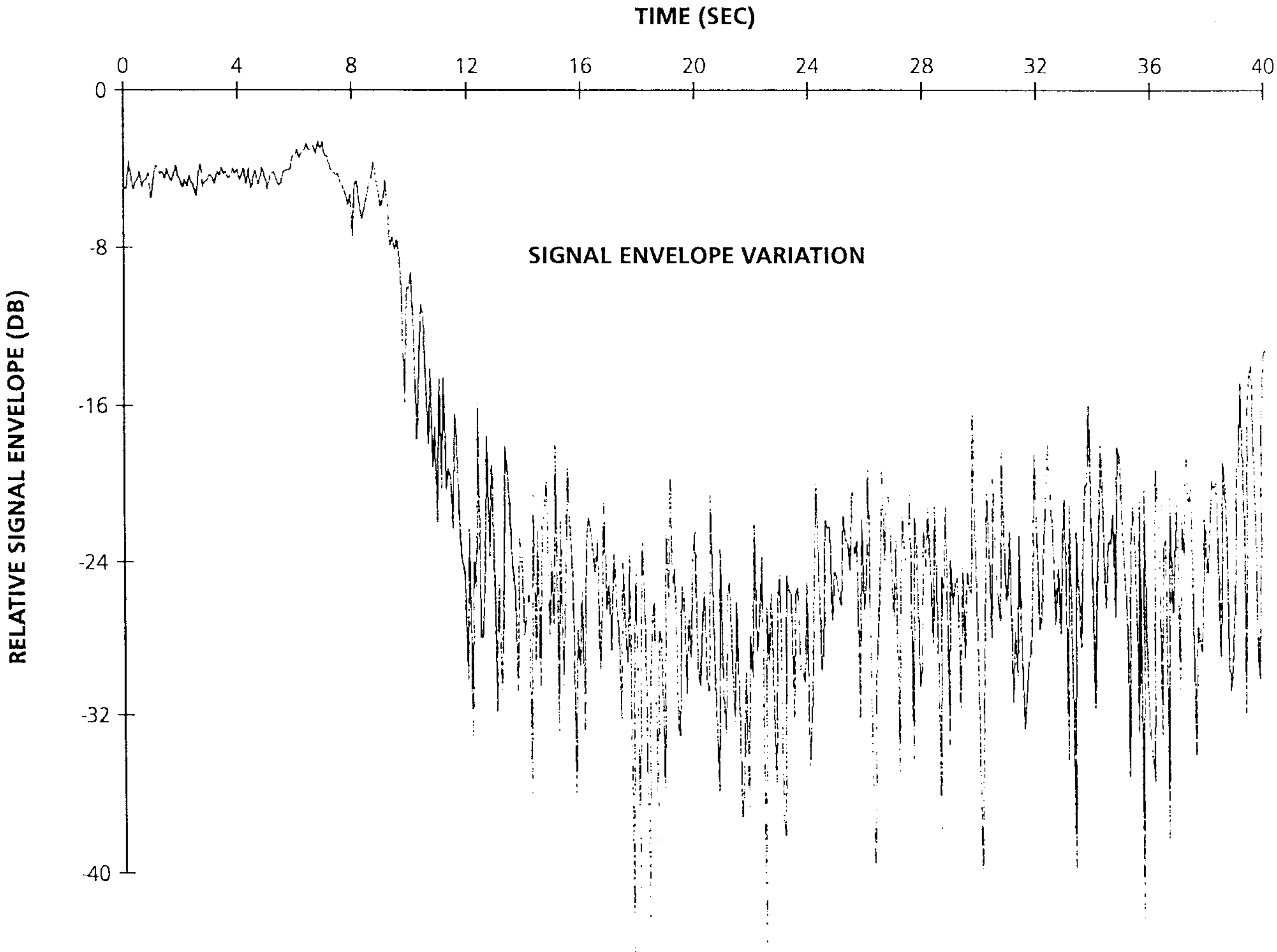

Fig. 27. Signal envelope variation; open to heavy shadowing; 18.925 GHz.

communications at Ka-band, one also needs to take into account fading caused by weather conditions. For this reason, statistical models are obtained that exhibit dependency on weather conditions. For a fixed satellite communications channel whose characteristics depend on weather conditions, the results show that the signal envelope and signal phase can be modeled as Gaussian, and their expressions are given by (10) and (8), respectively

$$p_w(r) = 1/\left(\sqrt{2\pi}\sigma_w\right)\exp\left[-(r-m_w)^2/2\sigma_w^2\right]. \quad (10)$$

The signal phase and signal envelope caused by weather conditions are given in Tables 4 and 6, respectively. Modeling parameters for shadowing and multipath fading under several representative rural areas are given in Tables 7 and 8 for signal envelope and signal phase, respectively. Figs. 32 and 33 show a signal envelope and signal phase model and measurements for thundershower conditions. The results show that the signal envelope model compared to measurements is a good approximation for up to 99% of the time. Also, the results show that the signal phase probability distribution model and measurements are in excellent agreement. The results shown between models and measurements are a reasonably good engineering approximation. A typical signal fading spectrum at Ka-band is shown in Fig. 34.

For land mobile satellite communications modeling at Ka-band, one needs to take weather conditions into account, as well as fading and shadowing. With this in mind, it is reasonable to assume that the two fading processes, one caused by weather conditions and the other due to fading and shadowing, are independent. The combined signal envelope probability density function $p_T(r)$ is given by

$$p_T(r) = p_w(r) \cdot p(r) \quad (11)$$

with $p_w(r)$ and $p(r)$ given by (10) and (2), respectively. Similarly, for the combined signal phase model, $p_T(\phi)$ is given by

$$p_T(\phi) = p(\phi_w + \phi_m) \quad (12)$$

where $p(\cdot)$ is Gaussian and ϕ_w and ϕ_m are the signal phase caused by weather conditions and fading and shadowing, respectively. $p_T(\phi)$ is also Gaussian.

C. Hardware and Software Channel Simulators

There have been several hardware and software channel simulators developed for the land mobile satellite channel [72]–[75], [77].

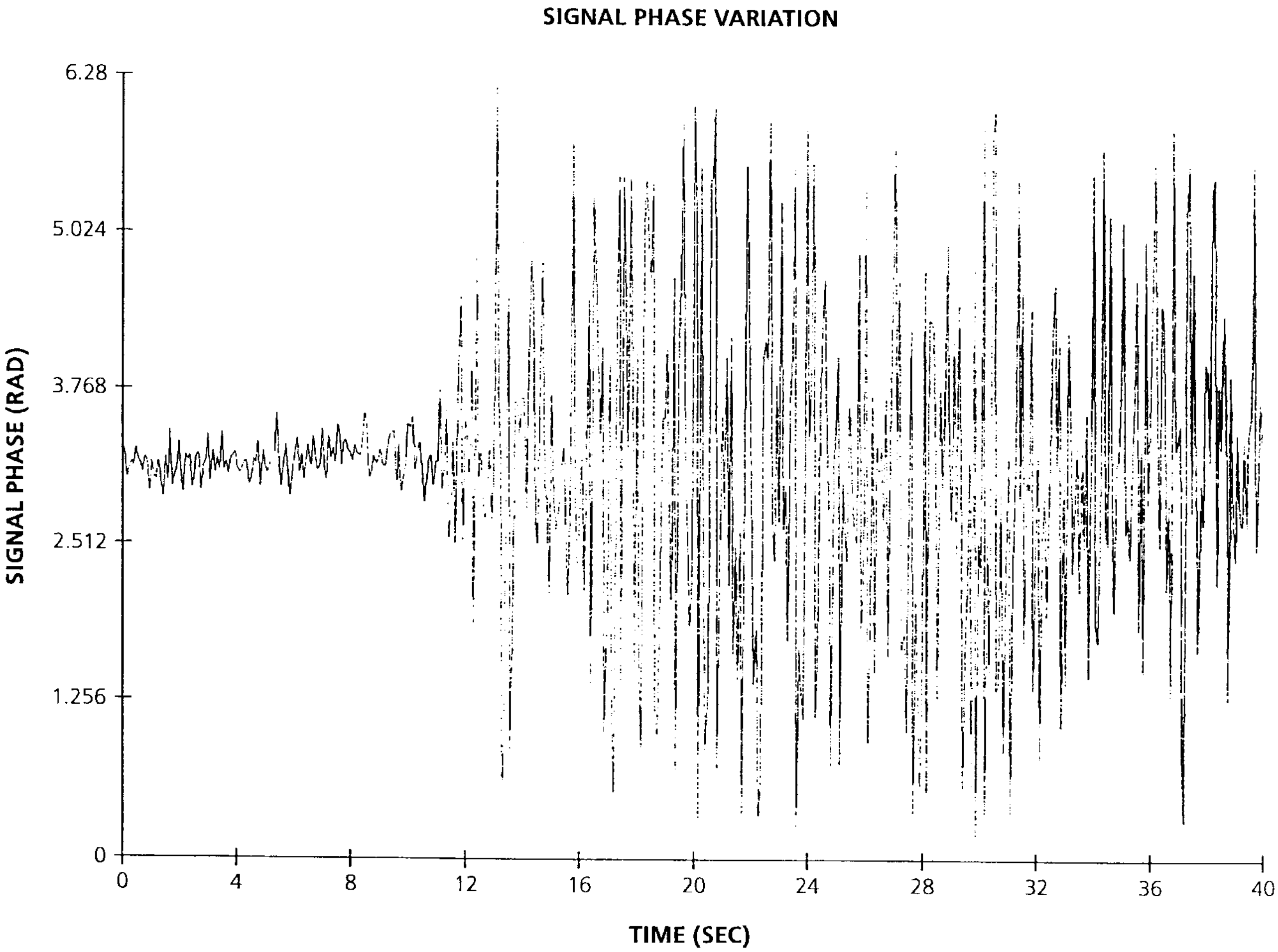

Fig. 28. Signal phase variation; open to heavy shadowing; 18.925 GHz.

Table 1 Phase Jitter and Random FM Under Light Shadowing Condition—870 MHz

Elevation Angle (deg)	rms Phase Jitter (deg)	rms Random FM (Hz)
20	12.8	5.5
15	8.1	3.9
5	19.8	9.1

Table 2 Phase Jitter and Random FM Under Heavy Shadowing Condition—870 MHz

Elevation Angle (deg)	rms Phase Jitter (deg)	rms Random FM (Hz)
30	14.0	5.5
20	16.2	7.3
15	16.2	6.9
5	26.9	14.0

Table 3 Phase Jitter and Random FM at 20° Elevation—1542 MHz

Elevation Angle (deg)	rms Phase Jitter (deg)	rms Random FM (Hz)
light shadowing	20.6	39.3
heavy shadowing	29.8	60.0
suburban	19.8	45.0

However, the emphasis of this subsection is on computer-generated channel models and, in particular, on the one developed at CRC [75]. All computer models for the fading

Table 4 Fixed Satellite Channel Phase Models—Ka-Band

Weather Conditions	Phase Model Parameters	
	Mean	Variance
clear sky	0.0072	0.00357
cloudy	0.0086	0.00405
cumulus cloud	0.0154	0.00864
overcast	0.0274	0.00414
intermittent light rain	0.0088	0.00546
thunder shower	0.0068	0.00414
light snow	0.0088	0.00442
overcast with snow	0.0082	0.00459
blowing snow	0.0089	0.00435
ice pellets	0.0094	0.00544
rain	-0.0089	0.03077

channels described in this subsection are based on the manipulation of a white Gaussian random process. This process is approximated by a sum of sinusoids with random phase angle [78]. An expression for the Gaussian random process, $a(t)$ is given below [79]

$$a(t) = Re \sum_{k=-N/2}^{N/2} V_k \exp[j2\pi(f_c + kf_0)t + j\lambda_k] \quad (13)$$

where V_k is the amplitude and λ_k is a random phase angle uniformly distributed between 0 and 2π. N is the number

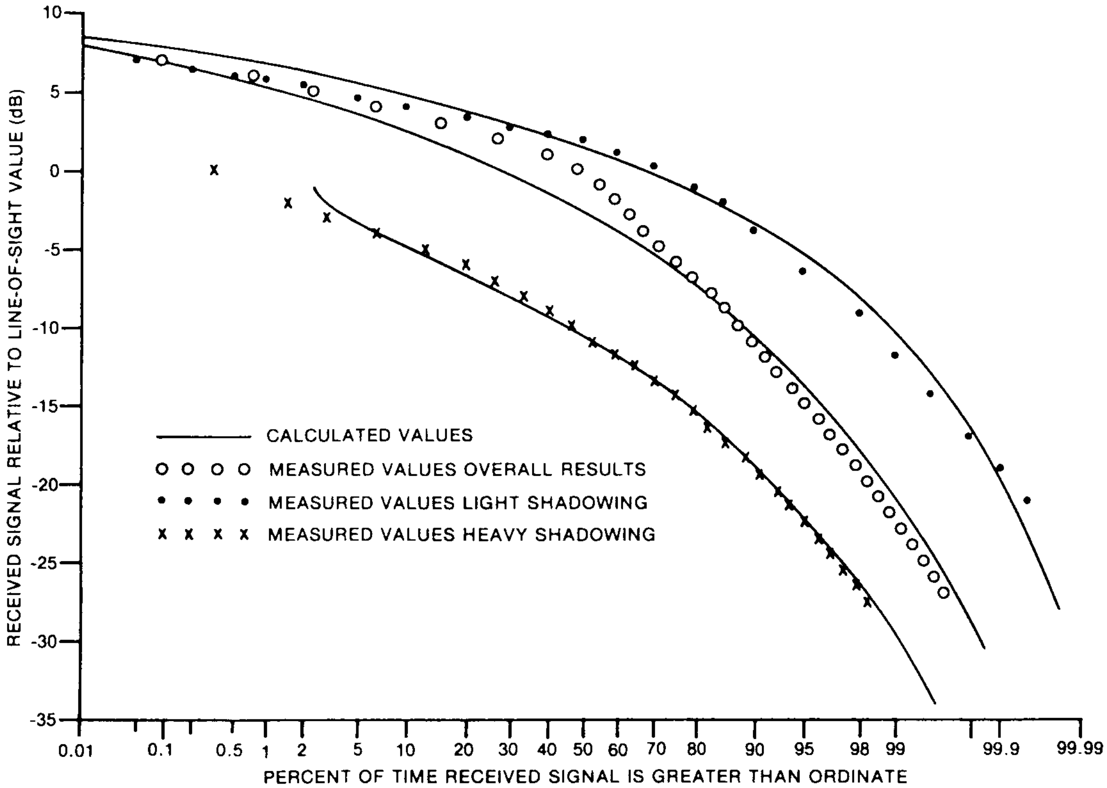

Fig. 29. A comparison of measured and calculated values of the probability distribution of signal envelope.

Table 5 Mobile Satellite Channel Envelope Models—L-Band

Channel Conditions	Envelope Model Parameters		
	μ	$\sqrt{d}$	b_0
infrequent light shadowing	0.115	0.115	0.158
frequent heavy shadowing	-3.914	0.806	0.063
overall results	-0.690	0.230	0.251

of sinusoids, $(f_c + kf_0)$ is the sinusoidal frequency, and Re denotes the "real part of."

The expression $a(t)$ can be rewritten as

$$a(t) = \mathrm{Re}\{[a_c(t) + ja_s(t)]\exp(j2\pi f_c t)\} \quad (14)$$

where

$$a_c(t) = \mathrm{Re}\sum_{k=-N/2}^{N/2} V_k \exp[j(2\pi k f_0 + \lambda_k)] \quad (15)$$

$$a_s(t) = \mathrm{Im}\sum_{k=-N/2}^{N/2} V_k \exp[j(2\pi k f_0 + \lambda_k)]. \quad (16)$$

Im denotes "the imaginary part of," $a_c(t)$, and $a_s(t)$ can be easily obtained using the FFT algorithm [80] for given V_k and λ_k.

1) Rayleigh Fading Channel: By definition [81], the envelope r of the two narrow-band Gaussian random processes is Rayleigh, and its phase ϕ is uniform. Therefore

$$r = \sqrt{a_c^2(t) + a_s^2(t)} \quad (17)$$

is Rayleigh and

$$\phi = \tan^{-1}\left(\frac{a_s(t)}{a_c(t)}\right) \quad (18)$$

is uniform.

2) Rician Fading Channel: When a fading process has a LOS component A_c together with multipath fading, the channel is modeled as Rician [82]. The Rice process is given by

$$a_r(t) = \mathrm{Re}\{[A_c + a_c(t) + ja_s(t)]\exp[j2\pi f_c t]\} \quad (19)$$

and its envelope r and phase ϕ are given by

$$r = \sqrt{[A_c + a_c(t)]^2 + a_s^2(t)} \quad (20)$$

$$\phi = \tan^{-1}\left(\frac{a_s}{A_c + a_c}\right). \quad (21)$$

3) Log-Normal Fading Channel: Local mean variation of a cellular mobile channel and shadowing caused by foliage attenuation are usually modeled as a log-normal fading process [46], [70], [83]. There are two methods of generating a log-normal fading process: one for slow fading and the other for fast fading.

a) Slow-fading log-normal process: The statistic of a log-normal process is generated from a normal (Gaussian) random process. For the slow-fading case, the normal random variate is generated from a nonlinear transformation

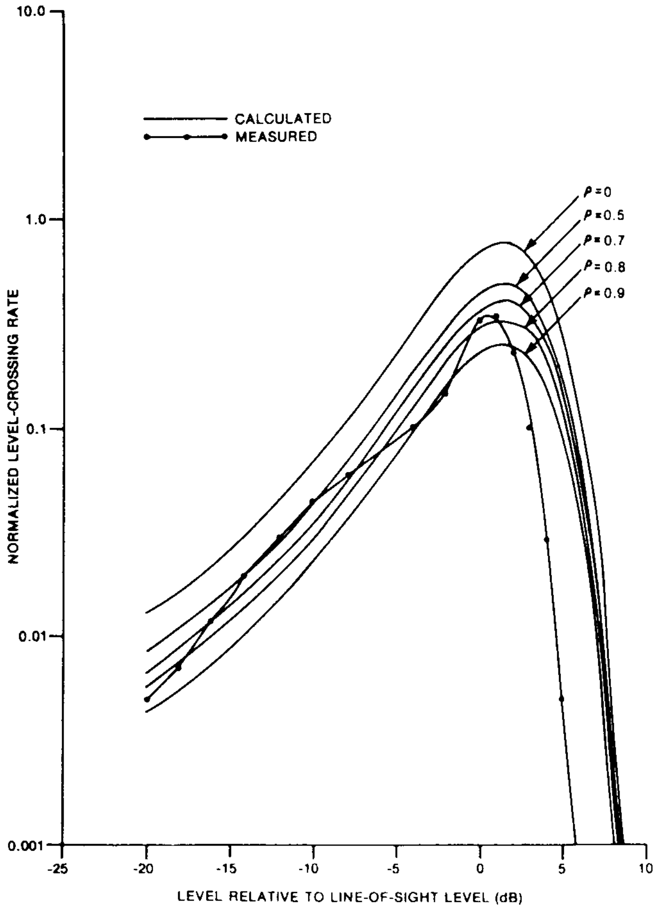

Fig. 30. LCR; infrequent light shadowing; 1542 MHz.

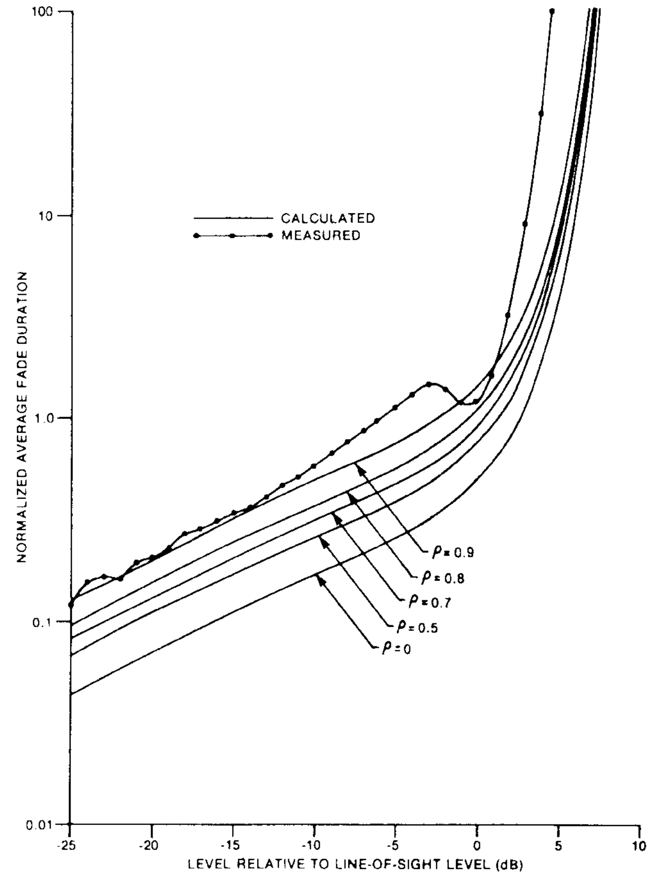

Fig. 31. AFD; infrequent light shadowing; 1542 MHz.

of a uniform distribution [84] and is given by

$$x_p = \sqrt{-2\ln u}\cos(2\pi v) \tag{22}$$

where u and v are uniformly distributed between zero and one. x_p is a Gaussian variate with zero mean and unity variance. To convert this variate to actual mean and variance, the following transformation is required:

$$x = \sqrt{d_0}x_p + \mu \tag{23}$$

where μ and d_0 are the mean and variance, respectively. The slow-fading log-normal process is given by

$$A_c = \exp[x]. \tag{24}$$

b) Fast-fading log-normal process: For the fast-fading log-normal model, the normal (Gaussian) process is approximated by a sum of sinusoids with random phase angle. The effect of the fading bandwidth is included. The fast log-normal model is given by

$$A(t) = \exp\left[\mu + \sqrt{d_0}x_c(t) + j\sqrt{d_0}x_s(t)\right] \tag{25}$$

where $x_c(t)$ and $x_s(t)$ are narrow-band Gaussian random processes, which can be obtained using expressions given in (15) and (16) with appropriate amplitude and phase.

Table 6 Fixed Satellite Channel Envelope Models—Ka-Band

Weather Conditions	Envelope Model Parameters	
	Mean*	Variance
clear sky	0.413	0.00087
cloudy	0.498	0.00025
cumulus cloud	0.346	0.00272
overcast	0.440	0.00041
intermittent light rain	0.483	0.00003
thunder shower	0.436	0.01386
light snow	0.488	0.00034
overcast with snow	0.458	0.00039
blowing snow	0.500	0.00021
ice pellets	0.482	0.00062
rain	0.662	0.0200

* nominal signal envelope level is 1. volt

Table 7 Mobile Satellite Channel Envelope Models—Ka-Band

Channel Conditions	Envelope Model Parameters		
	μ	$\sqrt{d}$	b_0
light to medium shadowing	-0.230	0.0115	0.1585
medium to heavy shadowing	-2.30	0.046	0.10
heavy shadowing	-1.95	0.46	0.0398

Table 8 Mobile Satellite Channel Phase Models—Ka-Band

Channel Conditions	Phase Model Parameters	
	Mean	Variance
light to medium shadowing	0.0068	0.0262
medium to heavy shadowing	- 0.0144	0.1124
heavy shadowing	- 0.0111	0.1934

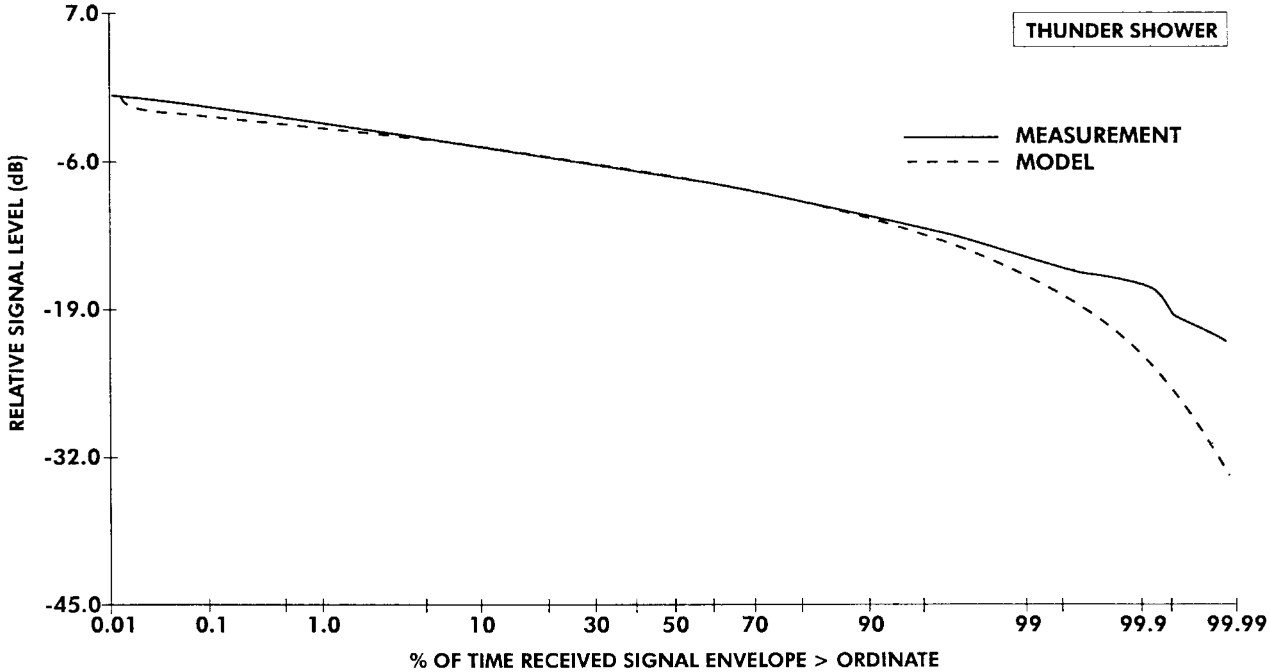

Fig. 32. Signal envelope model and measurement; thundershower conditions; 18.925 GHz.

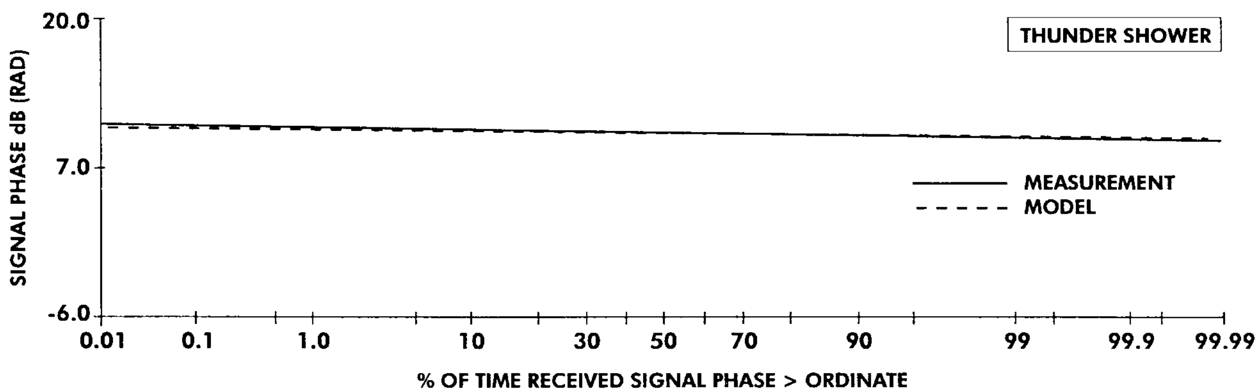

Fig. 33. Signal phase model and measurement; thundershower conditions; 18.925 GHz.

4) Land Mobile Satellite Fading Channel: This channel model [46] assumes that the LOS component under shadowing is log-normally distributed and that the multipath effect is Rayleigh distributed. The two process are additive. Thus, the channel model is given by the combination of log-normal and Rayleigh models described previously, as given below

$$a(t) = \mathrm{Re}\{[y_c(t) + a_c(t) + j(y_s(t) + a_s(t))] \exp[j2\pi f_c t]\}. \tag{26}$$

$a_c(t)$ and $a_s(t)$ are Gaussian random processes whose magnitude is related to the input sinusoid amplitude V_k of (15) and (16), which, in turn, is related to the multipath power b_0 as

$$b_0 = \sum_{k=1}^{N} V_k^2/2. \tag{27}$$

Similarly, $y_c(t)$ and $y_s(t)$ are log-normal random processes whose values are related in the following way. From (25), $A(t)$ can be rewritten as

$$\begin{aligned} A(t) &= y_c(t) + jY_s(t) \\ &= \exp\left[\mu\sqrt{d_0}\, x_c(t)\right] \\ &\quad \cdot \left[\cos\left(\sqrt{d_0}x_c(t)\right) + j\sin\left(\sqrt{d_0}x_s(t)\right)\right]. \end{aligned} \tag{28}$$

The values of $x_c(t)$ and $x_s(t)$ are related to the amplitude V_k of the sine waves of (15) and (16), with the x replacing the a. For this case, however, the power of the sum of the sine waves is normalized to unity, i.e.,

$$\sum_{k=1}^{N} V_k^2/2 = 1. \tag{29}$$

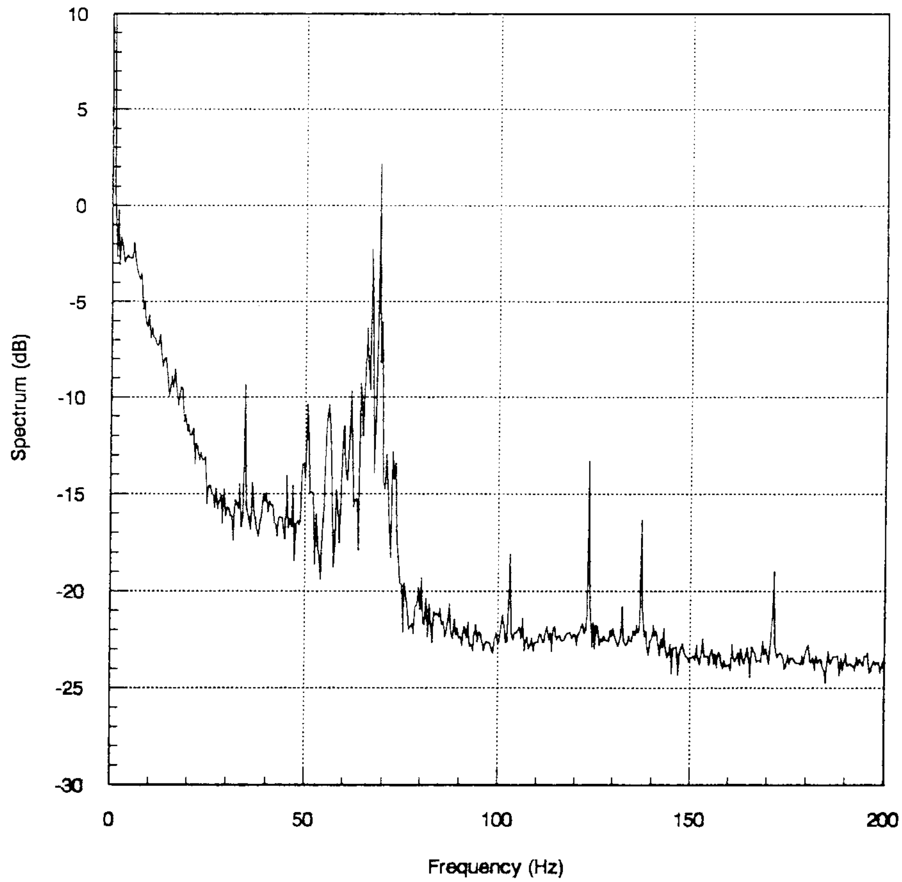

Fig. 34. A typical signal fading spectrum at Ka-band (18.925 GHz).

The signal envelope and signal phase are given by (30) and (31), respectively

$$r(t) = \sqrt{[y_c(t) + a_c(t)]^2 + [y_s(t) + a_s(t)]^2} \quad (30)$$

$$\phi(t) = \tan^{-1}\left(\frac{y_s(t) + a_s(t)}{y_c(t) + a_c(t)}\right). \quad (31)$$

5) Shaping of the Fading Spectrum: Two spectral shaping filters are used to shape the fading spectrum of the computer-generated models. One shaping filter is based on the land cellular mobile channel [70], [83] and the other has a Butterworth frequency response in the passband [75].

Numerical results in terms of the probability distribution of the computer models and analytical models [46] are shown in Fig. 35. The two results are in good agreement throughout the range of signal levels. A sample size of 240 000 has been used to obtain these probability distributions. Results on LCR and AFD, as well as other fading channel models, can be found in [75]. These channel models should facilitate the study of communication systems performance, especially on modulation schemes and coding strategy.

IV. Conclusion

This paper has presented a review on the progress of land mobile satellite communications channel measurements and modeling. Results highlighted were due to the efforts of many investigators worldwide. Various platforms, such as balloons, helicopters, airplanes, and communications satellites, were used to conduct propagation measurements at various elevation angles for channel characterization. Much data have been collected, ranging from UHF-band (800 MHz) to Ka-band (20/30 GHz), as indicated by numerous references given in this paper.

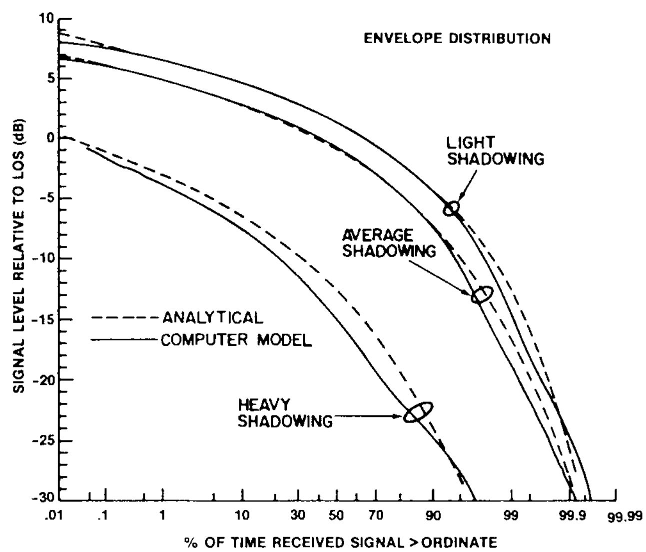

Fig. 35. Computer models with three-pole Butterworth shaping filter for fast light, average, and heavy shadowing signal envelope.

There were several statistical models developed to represent a land mobile satellite channel, as cited in the references. However, a statistical model developed by Loo at CRC was selected for detailed description. The reason for this choice was based on practicality. This model can represent most known fading conditions, such as Rician, log-normal, and Rayleigh. In addition, this model is physically intuitive, and it has compared reasonably well with measured data. Similarly, computer-generated models were also based on the model developed by Loo. Last, this paper should serve as a handy reference to any reader who is interested in the propagation characteristics of the land mobile satellite communications channel.

Acknowledgment

The authors wish to thank A. D. Kucar of 4U Communications Research, Inc., and E. J. Hayes for their suggestions and encouragement. They also thank E. E. Matt, M. Dufour, R. Yank, C. Pike, W. Janssen, and the Satcom Application Group, together with many co-op and career-oriented summer employment program students from Canadian universities, for their contributions in carrying out this work.

References

[1] M. Wachira, "Domestic mobile satellite systems in North America," in *Proc. Int. Mobile Satellite Conf.*, 1990, pp. 19–27.

[2] G. R. Egan and D. J. Sward, "Satellite mobile data service for Canada," in *Proc. Int. Mobile Satellite Conf.*, 1990, pp. A15–A19.

[3] A. Pedersen, "MSAT wide-area fleet management: End-user requirements and applications," in *Proc. Int. Mobile Satellite Conf.*, 1995, pp. 158–163.

[4] W. B. Garner, "The American mobile satellite system," in *Proc. Int. Mobile Satellite Conf.*, 1990, pp. 28–31.

[5] G. A. Johanson, N. G. Davies, and W. R. H. Tisdale, "Implementation of a system to provide mobile satellite services in North America," in *Proc. Int. Mobile Satellite Conf.*, 1993, pp. 279–284.

[6] M. Wagg, "Mobilesat, Australia's own," in *Proc. Int. Mobile Satellite Conf.*, 1990, pp. 3–7.

[7] K. Dinh, N. Hart, and S. Harrison, "Technical development for Australia's Mobilesat system," in *Proc. Int. Mobile Satellite Conf.*, 1990, pp. 213–218.

[8] M. Wagg and M. Jansen, "MobileSat, a characteristically Australian MSS," in *Proc. Int. Mobile Satellite Conf.*, 1995, pp. 404–408.

[9] R. E. Anderson and O. S. Roscoe, "How MSAT came about," in *Proc. Int. Mobile Satellite Conf.*, 1997, pp. 3–9.

[10] J. S. Butterworth, "Propagation measurements for land-mobile satellite services in the 800 MHz band," Communications Research Centre, Ottawa, Ont., Canada, Tech. Note 724, Aug. 1984.

[11] J. S. Butterworth, "Propagation measurements for land-mobile satellite systems at 1542 MHz," Communications Research Centre, Ottawa, Ont., Canada, Tech. Note 723, Aug. 1984.

[12] G. C. Hess, "Land-mobile satellite excess path loss measurements," *IEEE Trans. Veh. Technol.*, vol. VT-29, pp. 290–297, May 1980.

[13] E. Lutz, D. Cygan, M. Dippold, F. Dolainsky, and W. Papke, "The land mobile satellite communications channel-recording, statistics, and channel model," *IEEE Trans. Veh. Technol.*, vol. 40, no. 2, pp. 375–386, May 1991.

[14] W. J. Vogel and J. Goldhirsh, "Tree attenuation at 869 MHz derived from remotely piloted aircraft measurements," *IEEE Trans. Antennas Propagat.*, vol. AP-34, pp. 1460–1464, Dec. 1986.

[15] J. Goldhirsh and W. J. Vogel, "Roadside tree attenuations at UHF for land mobile satellite systems," *IEEE Trans. Antennas Propagat.*, vol. AP-35, pp. 589–596, May 1987.

[16] W. J. Vogel and J. Goldhirsh, "Fade measurements at L-band and UHF in mountainous terrain for land mobile satellite systems," *IEEE Trans. Antennas Propagat.*, vol. 36, pp. 104–113, Jan. 1988.

[17] J. Goldhirsh and W. J. Vogel, "Mobile satellite systems fade statistics for shadowing and multipath from roadside trees at UHF and L-band," *IEEE Trans. Antennas Propagat.*, vol. 37, pp. 489–498, Apr. 1989.

[18] W. J. Vogel and U.-S. Hong, "Measurement and modeling of land mobile satellite propagation at UHF and L-band," *IEEE Trans. Antennas Propagat.*, vol. 36, pp. 707–719, May 1988.

[19] W. J. Vogel and J. Goldhirsh, "Mobile satellite system propagation measurements at L-band using Marecs-B2," *IEEE Trans. Antennas Propagat.*, vol. 38, pp. 259–264, Feb. 1990.

[20] W. J. Vogel, J. Goldhirsh, and Y. Hase, "Land-mobile satellite fade measurements in Australia," *J. Spacecraft Rockets*, vol. 29, pp. 123–128, Jan.–Feb. 1992.

[21] J. Goldhirsh and W. J. Vogel, "Propagation effects for land mobile satellite systems: Overview of experimental and modeling results," NASA Ref. Pub., vol. 1274, Feb. 1992.

[22] W. J. Vogel and J. Goldhirsh, "Multipath fading at L band for low elevation angle, land mobile satellite scenarios," *IEEE J. Select. Areas Commun.*, vol. 13, pp. 197–204, Feb. 1995.

[23] W. J. Vogel, G. W. Torrence, and H.-P. Lin, "Simultaneous measurements of L and S-band tree shadowing for space-earth communications," *IEEE Trans. Antennas Propagat.*, vol. 43, pp. 713–719, July 1995.

[24] V. S. M. Renduchintala, H. Smith, J. G. Gardiner, and I. Stromberg, "Communications service provision to land mobile in northern Europe by satellite in high elevation orbits-propagation aspects," in *Proc. IEEE Vehicular Technology Conf.*, May 1990, pp. 706–713.

[25] G. Butt, B. G. Evans, and M. Richaria, "Narrowband channel statistics from multiband propagation measurements applicable to high angle land mobile satellite systems," *IEEE J. Select. Areas Commun.*, vol. 10, pp. 1219–1226, Oct. 1992.

[26] H. Smith, J. G. Gardiner, and S. K. Barton, "Measurements on the satellite channel at L and S bands," in *Proc. Int. Mobile Satellite Conf.*, 1993, pp. 319–324.

[27] A. Benarroch and L. Mercader, "Signal statistics obtained from a LMSS experiment in Europe with the Marecs satellite," *IEEE Trans. Commun.*, vol. 42, pp. 1264–1269, Feb./Mar./Apr. 1994.

[28] A. Kanatas, N. Papadakis, P. Chatzopoulos, T. Sofos, and P. Constantinou, "Land-mobile satellite channel measurements in Athens city center at 1800 MHz," in *Proc. Int. Mobile Satellite Conf.*, 1997, pp. 169–175.

[29] S. Yamamoto, E. Okamoto, A. A. Aboudebra, and T. Ikegami, "Propagation measurements for land mobile satellite communications at S-band with nongeo ETS-VI satellite," in *Proc. Int. Mobile Satellite Conf.*, 1997, pp. 177–182.

[30] Y. Matsumo, R. Suzuki, K. Kondo, and M. H. Khan, "Land mobile satellite propagation experiments in Kyoto city," *IEEE Trans. Aerosp. Electron. Syst.*, vol. 28, pp. 718–727, July 1992.

[31] N. Obara, K. Tanaka, S. Yamamoto, and H. Wakana, "Land mobile satellite propagation measurements in Japan using ETS-V satellite," in *Proc. Int. Mobile Satellite Conf.*, 1993, pp. 313–318.

[32] T. Ikegami, Y. Arakaki, H. Wakana, and R. Suzuki, "Measurement of multipath delay profile in land mobile satellite channels," in *Proc. Int. Mobile Satellite Conf.*, 1993, pp. 331–336.

[33] Y. Hase, W. J. Vogel, and J. Goldhirsh, "Fade-duration derived from land mobile satellite measurements in Australia," *IEEE Trans. Commun.*, vol. 39, pp. 664–668, May 1991.

[34] M. Yoshikawa and M. Kagohara, "Propagation characteristics in land mobile satellite systems," in *Proc. IEEE Veh. Technol. Conf.*, 1989, pp. 550–556.

[35] A. Bundrock and R. Harvey, "Propagation measurements for an Australian land mobile satellite system," in *Proc. Int. Mobile Satellite Conf.*, 1988, pp. 119–124.

[36] W. J. Vogel and J. Goldhirsh, "Earth-satellite tree attenuation at 20 GHz: Foliage effects," *Electron. Lett.*, vol. 29, no. 18, pp. 1640–1641, Sept. 1993.

[37] C. Loo, "Land mobile satellite channel measurement at Ka band using Olympus," in *Proc. IEEE Veh. Technol. Conf.*, 1994, pp. 919–923.

[38] E. Damosso, G. D. Bernardo, A. L. Rallo, M. Sforza, and L. Stola, "Propagation models for the land mobile satellite channel: Validation aspects," in *Proc. 1st Eur. Workshop Mobile/Personal Satcoms (EMPS'94)*, London, 1994, pp. 263–276.

[39] F. Murr, B. Arbesser-Rastburg, and S. Buonomo, "Land mobile satellite narrowband propagation campaign at Ka band," in *Proc. Int. Mobile Satellite Conf.*, 1995, pp. 134–138.
[40] D. S. Pinck and M. Rice, "K/Ka band channel characterization for mobile satellite systems," in *Proc. Int. Mobile Satellite Conf.*, 1995, pp. A-3 to A-10. See also *Proc. IEEE Veh. Technol. Conf.*, 1995, pp. 981–985.
[41] M. Rice, J. Slack, and B. Humpherys, "K-band land mobile satellite channel characterization using ACTS," *Int. J. Satellite Commun.*, vol. 14, pp. 283–296, 1996.
[42] L. Borghino, S. Buonomo, L. D'Amato, and C. Molinari, "Measurements and analysis on Ka land mobile satellite channel," in *Proc. 2nd Eur. Workshop Mobile/Personal Satcoms (EMPS'96)*, London, 1996, pp. 456–473.
[43] C. Loo, "Statistical models for land mobile and fixed satellite communications at Ka band," in *Proc. IEEE Veh. Technol. Conf.*, 1996, pp. 1023–1027.
[44] L. D'Amato, P. Ossola, and S. Buonomo, "Statistical analysis of attenuation measurements due to vegetation at 18 GHz," in *Proc. 2nd Ka Band Utilization Conf.*, Sept. 1996, pp. 407–414.
[45] S. Buonomo, L. D'Amato, and B. Arbesser-Rastburg, "Mobile propagation measurements at Ka band: Statistical results," in *Proc. 2nd Ka Band Utilization Conf.*, Sept. 1997, pp. 121–125.
[46] C. Loo, "A Statistical model for a land mobile satellite link," *IEEE Trans. Veh. Technol.*, vol. VT-34, pp. 122–127, Aug. 1985.
[47] ——, " Measurements and models of a land mobile satellite channel and their applications to MSK signals," *IEEE Trans. Veh. Technol.*, vol. VT-36, pp. 114–121, Aug. 1987.
[48] R. M. Barts, W. L. Stutzman, W. T. Smith, R. S. Schmier, and C. W. Bostian, "Land mobile satellite propagation modeling," *IEEE Int. Symp. Dig. Antennas Propagation*, June 1987, vol. 1, pp. 20–23.
[49] R. M. Barts and W. L. Stutzman, "Propagation modeling for land mobile satellite systems," in *Proc. Mobile Satellite Conf.*, May 1988, pp. 95–100.
[50] W. L. Stutzman, Ed., "Mobile satellite propagation measurements and modeling: A review of results for system engineers," in *Proc. Mobile Satellite Conf.*, pp. 107–117, May 1988.
[51] A. Benarroch and L. Mercader, "LMSS propagation model based on a European experiment using Marecs satellite," *Electron. Lett.*, vol. 27, no. 4, pp. 298–300, Feb. 1991.
[52] H. Wakana, "A propagation model for land mobile satellite communications," *IEEE Int. Symp. Dig. Antennas Propagation*, 1991, vol. 3, pp. 1526–1529.
[53] J. P. Castro, Statistical observations of data transmission over land mobile satellite channels," *IEEE J. Select. Areas Commun.*, vol. 10, pp. 1227–1235, Oct. 1992.
[54] R. M. Barts and W. L. Stutzman, "Modeling and simulation of mobile satellite propagation," *IEEE Trans. Antennas Propagat.*, vol. 40, pp. 375–382, Apr. 1992.
[55] B. Vucetic and J. Du, "Channel modeling and simulation in satellite mobile communication systems," *IEEE J. Selected Areas Commun.*, vol. 10, pp. 1209–1218, Oct. 1992.
[56] G. Butt, M. A. N. Parks, and B. G. Evans, "Narrowband and wideband characterization of satellite/PCN channel," in *Proc. Int. Mobile Satellite Conf.*, 1995, pp. 128–133.
[57] A. Jahn, S. Buonomo, M. Sforza, and E. Lutz, "A Wideband channel model for land mobile satellite systems," in *Proc. Int. Mobile Satellite Conf.*, 1995, pp. 122–127.
[58] A. G. Kanatas, E. C. Kanderakis, and P. Constantinou, "Narrowband land mobile satellite channel modeling," in *Proc. Int. Mobile Satellite Conf.*, 1995, pp. 109–114.
[59] Y.-S. Liu, "Modeling and simulation of a Ka band DBPSK/DQPSK mobile satellite channel," *Int. J. Satellite Commun.*, vol. 13, pp. 199–206, 1995.
[60] A. G. Kanatas and P. Constantinou, "Narrowband characterization of the land mobile satellite channel: A comparison of empirical models," *Eur. Trans. Telecommun. (AEI)*, vol. 7, no. 4, pp. 315–321, July/Aug. 1996.
[61] F. Dosiere, G. Maral, and J.-P. Boutes, "Shadowing process models for mobile and personal satellite systems," in *Proc. IEEE Global Telecommun. Conf.*, 1995, pp. 536–540.
[62] J. Goldhirsh and W. J. Vogel, "An extended empirical roadside shadowing model for estimating fade distributions from UHF to K-band for mobile satellite communications," *Space Commun.*, vol. 13, pp. 225–237, 1995.
[63] G. E. Corazza and F. Vatalaro, "A statistical model for land mobile satellite channel and its application to nongeostationary orbit systems," *IEEE Trans. Veh. Technol.*, vol. 43, pp. 738–742, Aug. 1994.
[64] F. Davarian, S. Chen, and M. Shihabi, "Channel behavior and power control in handheld mobile satellite links," in *Proc. Int. Mobile Satellite Conf.*, 1997, pp. 219–227.
[65] S.-H. Hwang, K.-J. Kim, J.-Y. Ahn, and K.-C. Whang, "A channel model for nongeostationary orbiting satellite system," in *Proc. IEEE Veh. Technol. Conf.*, 1997, pp. 41–45.
[66] S.-C. Ko, J. Kim, and C.-Y. Yang, "Practical channel simulation model for nongeo land mobile satellite (LMS) communications," in *Proc. IEEE Vehicular Technology Conf.*, 1997, pp. 411–415.
[67] J. Hagenauer and W. Papke, "Data transmission for maritime and land mobile using stored channel simulation," in *IEEE Vehicular Technology Conf. Rec.*, 1982, pp. 379–383.
[68] J. S. Butterworth and E. E. Matt, "The characterization of propagation effects for land mobile satellite services," in *Proc. Inst. Elect. Eng. Satellite Systems for Mobile Communications Navigation Conf.*, Conf. Pub. 222, 1983, pp. 51–54.
[69] R. W. Huck, J. S. Butterworth, and E. E. Matt, "Propagation measurements for land mobile satellite services," in *IEEE Vehicular Technology Conf. Rec.*, May 1983, pp. 265–268.
[70] W. C. Y. Lee, *Mobile Communications Engineering*. New York: McGraw-Hill, pp. 69–73, 169–177, 1982.
[71] P. Beckmann, *Probability in Communication Engineering*. New York: Harcourt, Bruce and Wold, 1967, pp. 124–126.
[72] J. Bodie, "A mobile communications channel simulator," Miller Communications Systems, Ltd., Kanata, Ont., Canada, 1984.
[73] F. Davarian, "Channel simulation to facilitate mobile satellite communications research," *IEEE Trans. Commun.*, vol. COM-35, pp. 47–56, Jan. 1987.
[74] R. M. Barts, J. Kim, R. Porter, T. Pratt, W. L. Stutzman, and C. W. Bostian, "Mobile satellite system performance through simulation," in *IEEE Vehicular Technology Conf. Rec.*, 1990, pp. 701–705.
[75] C. Loo and N. Secord, "Computer models for fading channels with application to digital transmission," *IEEE Trans. Veh. Technol.*, vol. 40, pp. 700–707, Nov. 1991.
[76] Y.-S Liu, "Computer simulation techniques for a mobile satellite communication channel," *Int. J. Satellite Commun.*, vol. 14, pp. 361–371, 1996.
[77] Y. Li, M. Pätzold, U. Killat, and F. Lane, "An efficient deterministic simulation model for land mobile satellite channels," in *Proc. IEEE Vehicular Technology Conf.*, 1996, pp. 1028–1032.
[78] S. O. Rice, "Mathematical analysis of random noise," *Bell Syst. Tech. J.*, vol. 23, pp. 282–332, July 1944; and vol. 24, pp. 46–156, Jan. 1945.
[79] C. Loo, "TWT noise suppression due to the presence of a large saturating carrier," *Can. Elect. Eng. J.*, vol. 3, no. 4, pp. 14–16, 1978.
[80] J. W. Cooley and J. W. Tukey, "An algorithm for the machine calculation of complex Fourier series," *Math. Comput.*, vol. 19, no. 90, pp. 297–301, Apr. 1965.
[81] A. Papoulis, *Probability, Random Variables and Stochastic Process*. New York: McGraw-Hill, 1965.
[82] K. A. Norton, L. E. Vogler, W. V. Mansfield, and P. J. Short, "The probability distribution of the amplitude of a constant vector plus a Rayleigh distributed vector," *Proc. IRE*, vol. 43, pp. 1354–1361, Oct. 1955.
[83] W. C. Jakes, Ed., *Microwave Mobile Communication*. New York: Wiley, 1974.
[84] G. M. Dillard, "Generating random numbers have probability distribution occurring in signal detection problems," *IEEE Trans. Inform. Theory*, vol. IT-13, pp. 616–617, Oct. 1967.
[85] C. J. Pike, D. R. Bradely, and D. J. Hindson, "Canadian EHF (28/19 GHz) satellite communication terminals for the Olympus program," in *Proc. Canadian Satellite User Conf.*, June 1989, pp. 364–369.
[86] C. J. Pike, "EHF (28/19 GHz) suitcase satellite terminal," in *Proc. Olympus Utilization Conf.*, Sevilla, Spain, Apr. 1993, pp. 203–207.
[87] C. Loo, E. E. Matt, J. S. Butterworth, and M. Dufour, "Measurements and modeling of land-mobile satellite signal statistics," in *Proc. IEEE Vehicular Technology Conf.*, May 1986, pp. 262–267.
[88] C. Loo, "Digital transmission through a land mobile satellite channel," *IEEE Trans. Commun.*, vol. 38, pp. 693–697, May 1990.

Chun Loo (Senior Member, IEEE) received the B.Eng. degree in electrical engineering from McGill University, Montreal, Canada, in 1962 and the M.S. degree in electrical engineering from the University of Ottawa, Ontario, Canada, in 1966.

From 1962 to 1965, he was with Computing Devices of Canada, Ottawa, where he participated in the development of avionic equipment. From 1966 to 1970, he was with Northern Electric R&D Labs (Bell Northern Research, now Nortel), where he was engaged in the theoretical studies of frequency modulation (FM) distortion and FM threshold characteristics and in computer simulation of communications systems. Since 1970, he has been with the Communications Research Centre, Industry, Canada (formally Department of Communications) as a Research Scientist. He has done systems analysis under the CTS (Hermes) project, a forerunner of direct broadcast satellite, and the ANIK B Pilot. He is the author of several papers relating to FM and digital transmission through a nonlinear satellite channel and on modeling of the land mobile satellite link. He developed a statistical model for the land mobile satellite channel that is widely in use by the research community worldwide. He has done systems studies on various modulation schemes for land mobile satellite communications applicable to the MSAT Program. He currently is a Senior Research Scientist conducting advanced system studies for future satellite communications, particularly, on satellite "onboard" processing and on characterization of the Ka-band satellite communication channel. He is a Principal Investigator on the project of onboard processing techniques under the Major Project on Broadband Satellite Communications of the Canadian Institute for Telecommunications Research.

Mr. Loo is a member of the Professional Engineers of Ontario, Canada.

John S. Butterworth received the B.Eng. and M.Eng. degrees in electrical engineering from Sheffield University, England, in 1959 and 1962, respectively.

He began work at the Canadian government's Communications Research Centre (CRC) in 1966 and has worked in the field of satellite communications ever since. He worked on Telesat's Anik A1 program, the CTS/Hermes program, and the mobile communications satellite MSAT. In preparation for the MSAT program, he was responsible for conducting a radio propagation research program using both simulated satellite sources and Inmarsat's MARECS satellite. In recent years, he was the Director of CRC's Satellite Applications and Projects division. Currently, he is managing the satellite communications portfolio in the development of Canada's next long-term space plan.